

## MASS TRANSPORT IN BIOREACTORS FOR COAL SYNTHESIS GAS FERMENTATION

K. T. Klasson, M. D. Ackerson, E. C. Clausen, and J. L. Gaddy  
Department of Chemical Engineering  
University of Arkansas  
Fayetteville, AR 72701

Keywords: Synthesis gas, bioreactors, hydrogen

### INTRODUCTION

Synthesis gas, a mixture of primarily CO, H<sub>2</sub> and CO<sub>2</sub>, is a major building block in the production of fuels and chemicals. The gas is derived from non-gaseous raw materials such as coal, shale oil, tar sands, heavy residue and biomass. The composition of synthesis gas is dependent upon the raw materials used and the gasification process. Coal-derived gas is rich in CO and H<sub>2</sub>, with lower concentrations of CO<sub>2</sub> and CH<sub>4</sub> and traces of H<sub>2</sub>S and COS (1).

A wide variety of both liquid and gaseous fuels may be produced from synthesis gas using Fischer-Tropsch synthesis including light hydrocarbons (methane, ethane), fuel range hydrocarbon distillates and heavy waxes. The stoichiometry for product formation may be characterized by the empirical relation (2):



As is noted, about 2 moles of H<sub>2</sub> are required for every mole of CO.

Since typical synthesis gas is deficient in H<sub>2</sub>, a catalytic water gas shift conversion is used to adjust the H<sub>2</sub>/CO ratio:



This same reaction may be carried out biologically at ambient conditions with high yield using bacteria such as *Rhodospirillum rubrum* (3) or *Rhodospseudomonas gelatinosa* (4).

### Purpose

The purpose of this paper is to present laboratory data from continuous culture experiments for the conversion of H<sub>2</sub>O and CO in synthesis gas to CO<sub>2</sub> and H<sub>2</sub> using a biological process. The photosynthetic bacterium *R. rubrum* is employed. Performance results from continuous stirred tank and trickle-bed reactors are presented and discussed.

### BIOREACTOR DESIGN

The choice of a suitable bioreactor for synthesis gas fermentations is a matter of matching reaction kinetics with the capabilities of the various reactors. It has been found that for these slightly soluble gases, the rate

of mass transfer usually controls the reactor size (5,6). Mass transfer capabilities of the reactor must be balanced with the cell density achieved. The proper reactors for these systems will likely be ones that achieve high mass transfer rates and high cell densities. These concepts will be expanded in this and the following section.

### Gas-Liquid Mass Transfer Concepts

The transfer of gas phase substrates in fermentation systems involves three heterogeneous phases: the bulk gas phase, the culture medium (liquid) and microbial cells (solid) suspended in the medium. The reactants, present in the gas phase, must be transported across the gas-liquid interface and diffuse through the culture medium to the cell surface to be consumed by the microbes. In general, a combination of the following resistances can be expected (7):

1. Diffusion through the bulk gas to the gas-liquid interface.
2. Movement across the gas-liquid interface.
3. Diffusion of the solute through the relatively unmixed liquid region (film) adjacent to the bubble and into the well-mixed bulk liquid.
4. Transport of the solute through the bulk liquid to the stagnant film surrounding the microbial species.
5. Transport through the second unmixed liquid film associated with the microbes.
6. Diffusive transport across the liquid/solid boundary and into the microbial floc, mycelia, or particle, if appropriate. When the microbes take the form of individual cells, this resistance disappears.
7. Transport across the cell envelope to the intracellular reaction site.

As with the conventional chemical engineering analysis of absorption processes, mass transfer through the bulk gas phase is assumed to be instantaneous. Also, when individual cells are suspended in a medium, the liquid film resistance around the cells is usually neglected with respect to other resistances, because of the minute size and the enormous total surface of the cells (8). Thus, for the transfer of sparingly soluble gases, such as CO, the primary resistance to transport may be assumed to be in the liquid film at the gas-liquid interface.

It can be shown that the substrate transfer rate per unit of reactor volume,

$\frac{dN_S^G}{V_L dt}$ , is given in terms of the gas phase partial pressures as:

$$\frac{d N_S^G}{V_L dt} = \frac{K_L a}{H} (p_S^G - p_S^L) \quad (3)$$

where  $N_S^G$  = moles substrate transferred from the gas phase,  $V_L$  is the volume of the liquid phase,  $t$  is time,  $K_L$  is the overall mass transfer coefficient,

a is the gas-liquid interfacial area per unit volume, H is Henry's law constant,  $P_S^G$  is the partial pressure of the substrate in the bulk gas phase, and  $P_S^L$  is the partial pressure (dissolved tension) of the substrate in the liquid phase ( $P_S^L = HC_L$ ). The rate of transport from the gas phase must be equal to the rate of consumption in the liquid phase, given by a Monod relationship:

$$\frac{d N_S^G}{V_L dt} = \frac{X q_m P_S^L}{K'_p + P_S^L + (P_S^L)^2/W'} = \frac{K_L a}{H} (P_S^G - P_S^L) \quad (4)$$

where X is the cell concentration and  $q_m$ ,  $K'_p$ , and W' are Monod constants.

Equation (4) shows that a bioreactor for these gaseous systems must operate in either of two regimes. In one case, sufficient cells are present to react more solute, but the mass-transfer rate cannot keep pace. Therefore, the liquid phase concentration goes to zero and the reactor is mass transport limited. The cell concentration and rate of consumption are limited by the ability of that particular reactor to transfer substrate. In the other case, sufficient substrate can be supplied, but the cell concentration does not allow consumption at an equal rate. Then the liquid phase concentration is not zero (with possible inhibitory effects) and the rate is limited by the cell concentrations in that particular bioreactor. Obviously, the best bioreactor is one that will achieve high cell concentrations and high mass transfer rates.

#### Stirred Tank Reactor Studies

The traditional reactor used in continuous fermentation processes is the stirred tank reactor, or CSTR. As it relates to gas phase substrates, the CSTR has continuous gas flow into a constant volume liquid phase reactor. A small liquid feed stream is utilized to supply nutrients to the microorganisms in the reactor system and to remove products. The agitation rate in the system is relatively high in order to promote transfer of the sparingly soluble gas into the liquid culture medium.

Experiments have been carried out in a CSTR at different gas flow rates under mass transfer-limited conditions. In these experiments, the progress of the reaction is followed by the use of an inert component, whose partial pressure does not change throughout the system. Assuming perfect mixing in both the gas and the liquid phases, the CO uptake rate from the gas phase may be described by Equation (5) under mass transfer limiting conditions:

$$\dot{n}_I (Y_{CO}^I - Y_{CO}^O) = \frac{K_L a}{H} \cdot V_L \cdot P_{CO}^O \quad (5)$$

Equation (5) may be easily rearranged to yield:

$$\left( \frac{P_{CO}^I}{P_{CO}^O} - \frac{P_I^I}{P_I^O} \right) = \frac{K_L a}{H} \cdot \frac{V_L \cdot RT}{G^I} \quad (6)$$

A plot of CO conversion as a function of pseudo retention time in the CSTR (defined as the liquid volume in the reactor divided by the gas flow rate) is shown in Figure 1. As noted, a conversion of about 55 percent was attained at a retention time of 1 h. The maximum conversion was about 85 percent, attained at retention times of 3 h or above. Conversion in the CSTR is limited by the mixed flow pattern inside the reactor.

The mass transfer coefficient,  $K_{L,A}$ , may be obtained for the CSTR experiments by employing Equation (6). If the left hand side of Equation (6) is plotted as a function of  $V_L RT/HG$  a straight line should be obtained with a slope of  $K_{L,A}$  if the experiments are carried out under mass transfer limiting conditions. Such a plot is shown in Figure 2, where  $K_{L,A}$  is shown to have a value of  $70.0 \text{ h}^{-1}$ . It should be noted that these experiments were carried out at a constant agitation rate of 400 rpm. Agitation rate, impeller design and other physical characteristics of the reactor significantly affect the value of the mass transfer coefficient.

#### Trickle Bed Reactor Studies

Trickle-bed reactors are used conventionally to obtain a low pressure drop or low liquid holdup when there is practically no heat to remove or supply, or the liquid is corrosive. They are usually operated countercurrently since a higher driving force can be achieved than with cocurrent operation. However, when an irreversible reaction occurs between the dissolved gases and the absorbent (as in biological systems), the mean concentration driving force is the same for both modes of operation. In this case, the capacity of cocurrent columns is not limited by flooding and at any given flow rates of gas and liquid, the pressure drop in a cocurrent column is less (9).

Experiments were conducted in a cocurrent column packed with ceramic Intalox saddles. In this experimental setup, the liquid and the gas were disengaged in a liquid/gas separator with the culture being recirculated back to the top of the column. In this manner, a high concentration of cells can be maintained inside the reactor while at the same time using high L/G operating conditions inside the column. For this system, assuming perfect plug flow in the gas phase ascending through the column and constant partial pressure of the inert gas in the system (as closely substantiated from experimental data), the outlet ratio of CO to the inert can be related to other operating conditions according to the equation (10):

$$\ln \frac{Y_{CO}^i}{Y_{CO}^o} = K_{L,A}' \frac{ShRT}{HG} \quad (7)$$

A plot of CO conversion as a function of pseudo retention time in the trickle bed reactor is shown in Figure 3. In contrast to the CSTR results, nearly complete conversion was seen in the trickle bed at a retention time of 0.6 h. Complete conversion was obtained because the trickle bed operates very closely to ideal plug flow behavior.

Figure 4 shows the calculation of the mass transfer coefficient for the trickle bed as a rearrangement of Equation (7). The value of  $K_{L,A}$  of  $23.5 \text{ h}^{-1}$  is in good agreement with the value of  $27.0 \text{ h}^{-1}$  calculated from the results of Charpentier (9).

## CONCLUSIONS

The performance of *R. rubrum* in producing  $H_2$  was demonstrated in a continuous stirred tank reactor and a trickle-bed reactor. A conversion of 0.85 was obtained in the CSTR at a pseudo retention time of 3 h. The plug flow trickle-bed reactor gave a conversion of 100 percent at a retention time of only 0.6 h. Mass transfer coefficients were obtained for the two continuous reactors, with  $K_L a$  equaling  $70.0 \text{ h}^{-1}$  in the CSTR and  $23.5 \text{ h}^{-1}$  in the trickle-bed reactor.

## REFERENCES CITED

1. McCullough, G. R., Roberts, S. C. and Van der Burgt, M. J., "Shell Coal Gasification Process," *Energy Prog.*, 2, 69 (1982).
2. Schreiner, M. "Research Guidance Studies to Assess Gasoline from Coal by Methanol-to-Gasoline and Sasol-Type Fischer-Tropsch Technologies," Report No. FE-2447-13, U. S. Department of Energy, Washington, D.C. (1978).
3. Dashekvicz, M. P. and Uffen, R. L., "Identification of a Carbon Monoxide Metabolizing Bacterium as a Strain of *Rhodopseudomonas gelatinosa* (Molisch) van Niel," *Int. J. System. Bacteriol.*, 29, 145-148 (1978).
4. Uffen, R. L., "Anaerobic Growth of a *Rhodopseudomonas* Species in the Dark with Carbon Monoxide as the Sole Carbon and Energy Substrate," *Proc. Natl. Acad. Sci.*, 73, 3298-3302 (1976).
5. Vega, J. L., Clausen, E. C., and Gaddy, J. L., "Study of Gaseous Substrate Fermentations: Carbon Monoxide to Acetate, 1. Batch Cultures," *Biotechnol. Bioeng.*, 34, 774 (1989).
6. Vega, J. L., G. M. Antorrena, E. C. Clausen, and J. L. Gaddy, "Study of Gaseous Substrate Fermentations: Carbon Monoxide to Acetate. 2. Continuous Culture," *Biotechnol. Bioeng.* 34, 785 (1989).
7. Bailey, J. E. and D. F. Ollis, *Biochemical Engineering Fundamentals*, McGraw-Hill, New York (1986).
8. Finn, R. K., "Agitation-Aeration in the Laboratory and in Industry," *Bacteriol. Rev.*, 18, 154-274 (1954).
9. Charpentier, J. C., "Mass-Transfer Rate in Gas-Liquid Absorbers and Reactors," *Adv. Chem. Eng.*, 11, 1 (1981).
10. Antorrena, G. A., Internal Report, Department of Chemical Engineering, University of Arkansas, Summer 1987.

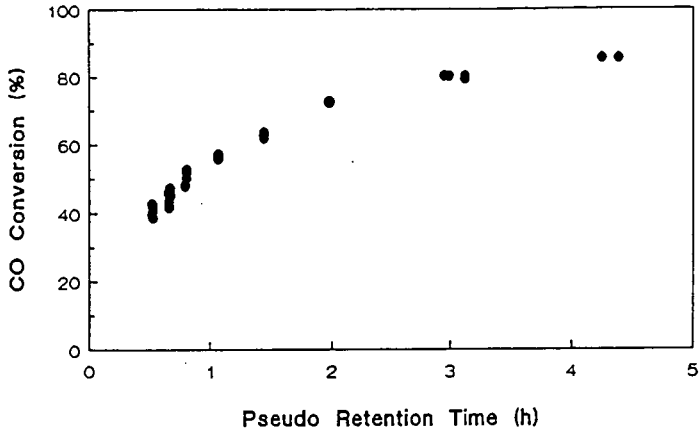


Figure 1. CO conversion profile in the CSTR at various pseudo retention times

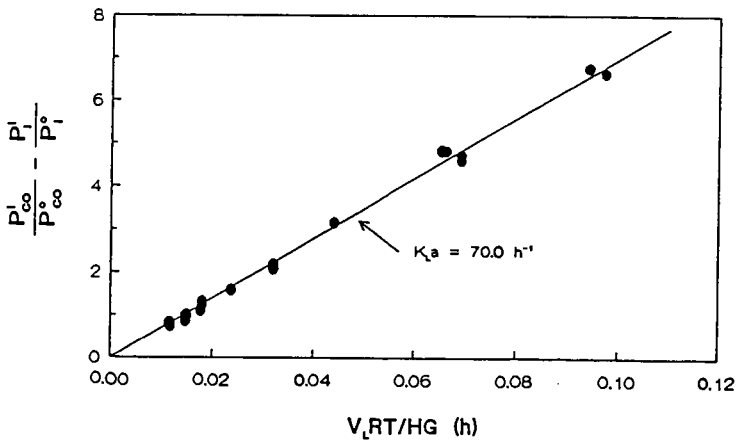


Figure 2. Determination of the mass transfer coefficient in the CSTR

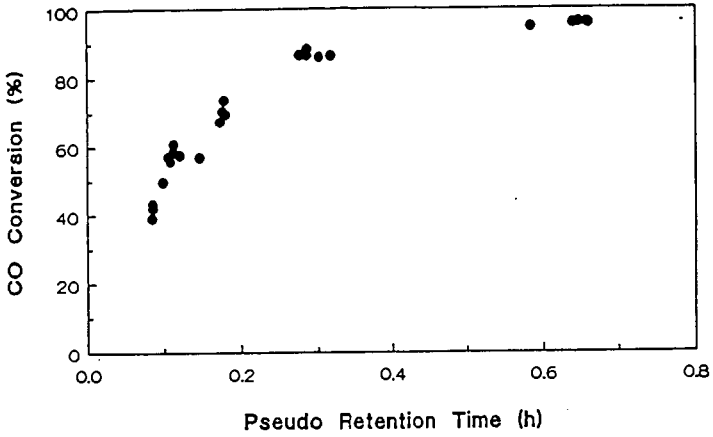


Figure 3. CO conversion profile in the trickle-bed reactor at various pseudo retention times.

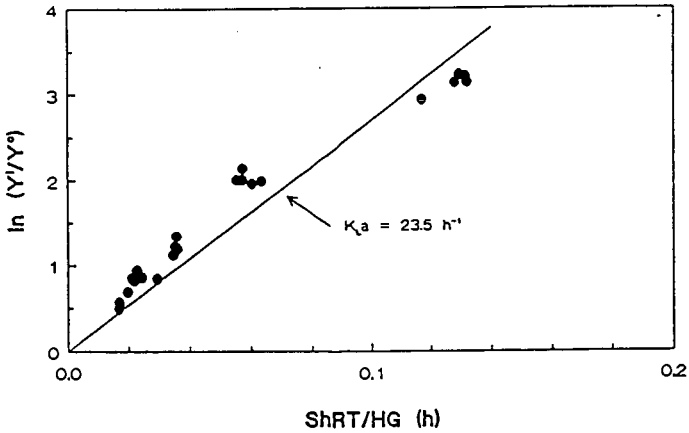


Figure 4. Determination of the mass transfer coefficient in the trickle-bed reactor

## EFFECT OF COAL PARTICLE SIZE ON VOLATILE YIELDS DURING RAPID HEATING

J. R. Gibbins, J. Jacobs\*, C. K. Man and K. J. Pendlebury.

Dept. of Mechanical Engineering, Imperial College of Science, Technology and Medicine, Exhibition Road, London, SW7 2BX.

\* Rheinisch-westfaelisch-technische Hochschule, Aachen, Germany.

### INTRODUCTION

Typically a wide range of particle sizes, with mean diameters between about 10 and 300  $\mu\text{m}$ , are present in feed coal streams to entrained flow combustion and gasification processes. The magnitude of any variation in volatile yield with particle size over this range is therefore relevant for computer modelling of such processes, and possibly specification of an optimum feed particle size distribution. The result will also affect the validity of coal characterisation measurements, made on a sample with a limited size range, for predicting the behaviour of a real coal feed.

Mass transport effects should result in a monotonic increase in volatile yields during rapid heating with decreasing particle size, due to the progressive reduction in retrograde char-forming reactions as the residence time of the nascent volatiles within the particles is reduced. In practice, however, the magnitude of such mass transfer effects may be difficult to measure in isolation. One possible source of interference is the differences in heating rate which will also occur between different-sized particles in tests in entrained flow reactors, another is the difficulty in obtaining different size cuts of a coal with identical mineral and maceral composition. The basic tendency will be for finer fractions to become enriched with the more friable constituents of the coal. Less uniform effects may result, however, from the behaviour of intrinsically-homogenous sub-components of a coal (e.g. fossil spores<sup>1</sup>). These may be released virtually intact from the coal matrix by grinding, but are then resistant to further comminution.

Since a captive-sample wire-mesh reactor was used in the present study, differences in heating rate between different size cuts were not considered to be a problem. Under the test conditions used (1000 K/s heating to 950°C) all of the samples softened in the early stages of heating, ensuring good heat transfer between the mesh and the sample. The temperature of the mesh in the area where the sample was distributed was computer-controlled to give typically better than  $\pm 20$  K compliance with the desired value.

To allow for the effect of compositional differences between size cuts a number of approaches were used in the present study.

- (a) The ash content of size fractions was measured and data reported on a daf basis to avoid interference from mineral enrichment.
- (b) Maceral analyses were performed to identify whether or not maceral enrichment had occurred during grinding.
- (c) A second grinding step, using the top size fraction tested as the starting material instead of the raw coal, was used to give more homogenous samples (see below for more details).
- (d) A vitrain sample with essentially homogenous (>90% vitrinite) starting composition, and thus largely immune to maceral enrichment effects, was also tested.

## EXPERIMENTAL

### Coal preparation

Samples of two U.K. bituminous coals (Daw Mill, type 802, and Kellingley, type 602) and one hand-picked Shirebrook Blackshale vitrain sample (>90% vitrinite) were obtained in lump form from British Coal's Technical Services and Research Executive (TSRE) at Bretby. The Pittsburgh No. 8 sample from the Argonne Premium Coal Sample programme<sup>2</sup> was also used.

The lump coal samples were ground to all <150 $\mu$ m using a Fritsch Pulverisette II motorised grinder with frequent sieving to remove undersize material. The Pittsburgh No. 8 was ground by hand. The ground coal was screened to produce the following size fractions: <38  $\mu$ m, 38-53  $\mu$ m, 53-75  $\mu$ m, 75-106  $\mu$ m and 106-150  $\mu$ m. The mass distributions from this first grinding process are shown in Table 1.

For the coals (which showed significant maceral enrichment effects) a second grinding stage was also used. The 150-106 $\mu$ m size fraction was divided into four equal sub-samples, using a Microscal spinning riffler. Three of these sub-samples were subsequently reground to all pass through 53, 75 and 106  $\mu$ m respectively, and then screened to give 38-53 $\mu$ m, 53-75  $\mu$ m and 75-106  $\mu$ m size cuts.

All samples were dried overnight in a nitrogen-purged oven at 105 °C and then stored under nitrogen until required.

### Sample analysis

Small samples of each of the coal fractions (approx. 0.5g) were mounted in a fast-setting 'Buehler Epo-thin' low viscosity resin. After polishing, maceral compositions were observed by examination under a light microscope. To obtain quantitative maceral data, 500 point counts were made on each sample.

Because of the limited amounts of sample available, a thermogravimetric analyser (TGA - Stanton Redcroft Model TG-780) was used to measure ash contents. Approx. 10 mg samples were heated at 30 °C min<sup>-1</sup> to 900 °C in N<sub>2</sub>/air.

### Wire-mesh apparatus

A version of the wire-mesh reactor previously developed at Imperial College<sup>3,4</sup> was used for devolatilization experiments. This incorporates a computer-based temperature control system, with a two-colour pyrometer for temperature measurements. All experiments were undertaken with a flowing helium sweep gas at atmospheric pressure and using a heating rate of 1000 K/s to 950°C, with 10 s hold at peak temperature. Previous work<sup>5</sup> has shown that volatile yields are insensitive to experimental variations in heating rate, temperature or hold time under these conditions.

The sample holder was made from folded AISI 304 stainless steel mesh (25  $\mu$ m wires x 32  $\mu$ m aperture). A 5-10 mg coal sample was spread within a 15 mm diameter circle at the centre of the sample holder, and total volatile yields were measured by direct weighing before and after experiments.

## RESULTS AND DISCUSSION

Total volatile yields and ash, vitrinite, liptinite and inertinite contents for the sized fractions of the coals from the first and second grinding stages and the vitrain are shown in Figs 1-4. Data points are included for the daf volatiles values to indicate the experimental scatter in the data, with lines drawn through the average values. Points are also shown for other quantities if only limited information is available.

Considering first the volatile yields on a dry basis for the 'first grind' size fractions of the coals, it is interesting to note that there appears to be relatively little effect of particle size. Thus, although differences in the grinding methods used make definitive general conclusions impossible, the results in Figs 1-3 do suggest that overall volatile release per unit mass from the different size fractions may be roughly constant under actual plant conditions (before any heating rate effects are taken into account).

Inspection of the ash contents for the coal size fractions shows, however, that this apparent invariance in dry volatile yields is the result of two opposing trends rather than of an underlying uniformity in coal behaviour! In line with previous findings<sup>6</sup> the ash contents of the size fractions generally increase with decreasing size. This then tends to counteract the general trend for an increase in volatile release from the organic constituents of the coal with decreasing size, as shown in the daf yields for the first grind size fractions.

Volatile yields on a daf basis from the first grind size fractions were not observed to increase monotonically, however, suggesting that a simple reduction in mass transfer resistance was not the only factor involved. This supposition is confirmed by the variation in maceral analysis between size fractions, although some allowance must be made for scatter in the maceral data (particularly at the smaller particle sizes when edge effects become more common with the point counting techniques used). No clear general trends for maceral enrichment emerge from the (somewhat limited) data presented, however, beyond a probable decrease in liptinite content for the smaller size fractions.

The significance of changes in maceral composition can be inferred from the results of previous work on maceral concentrates<sup>7</sup>. For similar UK coals and under similar experimental conditions, it was estimated that volatile yields from 'pure' vitrinite, liptinite and inertinite were of the order of 40%, 80% and 30% daf respectively. It was also found that in maceral mixtures (including whole coals and different maceral concentrates obtained by density separation), the contribution of individual maceral components to overall yields were simply additive.

In an attempt to allow the effect of mass transfer to be examined with less interference from maceral enrichment effects, a similar set of size fractions was prepared using the 106-150  $\mu\text{m}$  fraction from the first grind, instead of the raw coal, as the starting material. This method was at least partly successful. For the UK coals, ash levels in the samples are relatively constant and, particularly for the Kellingley samples, the overall trend in maceral levels is roughly level. Significant differences still exist in maceral contents for the Daw Mill coal, although the changes are now monotonic. The latter trends perhaps reflect more homogeneity within the individual maceral groups than occurred in the original coal, coupled with grindability differences. The limited data for the Pittsburgh No. 8 sample showed little effect of maceral enrichment in the second grind, but a much more pronounced, monotonic increase in ash content with decreasing particle size. Overall the second grinding strategy can probably be regarded as at least partly successful, in that monotonic changes in daf volatile yields with changing particle size were observed for these samples.

The effect of mass transfer is still not easy to resolve, however, from the second grind daf volatile data. For the Kellingley and Pittsburgh samples volatile yields increased with decreasing particle size, in line with expectations. For the Daw Mill samples no increase was observed, despite maceral changes that suggest that an increase in volatile yield should result even in the absence of any mass transfer effects.

Data from the vitrain samples, shown in Fig. 4, supports the existence of a small mass transfer effect. Two sets of samples were used, obtained by sieving after grinding to all pass 150  $\mu\text{m}$  and 300  $\mu\text{m}$  respectively. Because of the high vitrinite concentration in the original vitrain it was expected that maceral enrichment would not occur during grinding, although there is some evidence for slight enrichment in the limited data obtained. Interestingly, even with the small ash content of the original sample, high levels of ash enrichment occurred in the smaller size fractions from the -300  $\mu\text{m}$  grind. Nonetheless, daf volatile yields from the two sets of samples agreed closely in the overlapping region, despite the significantly different preparation procedures used, suggesting that maceral enrichment was not a major problem.

#### CONCLUSIONS

When interference from mineral and maceral enrichment effects was minimised, small increases in daf volatile yields for rapid heating have been observed with decreasing particle size. This is likely to result from reduced resistance to volatiles mass transfer within the smaller particles. Volatile yield increases varied from nearly zero to 8 percentage points between the 100-150  $\mu\text{m}$  and 38-53  $\mu\text{m}$  size fractions.

In practice, selective mineral and maceral enrichment of different size fractions is very difficult to prevent. Without special preparation procedures these enrichment effects can swamp any effect of changing mass transfer resistance.

In ground samples prepared from whole coals selective enrichment effects probably tend to offset mass transfer effects. Because of this, the simplifying assumption of invariant volatile yields with particle size, often made in combustion and gasification models, appears to be reasonably valid.

The unavoidability of maceral enrichment effects imposes a limit on the accuracy with which a characteristic rapid-heating volatile yield for a whole coal can be measured if, as is often the case, the test method used (e.g. wire-mesh, entrained flow reactor) requires a sample with a restricted size range. The present study indicates a potential uncertainty of about  $\pm 3$  percentage points in indicated daf values. More representative measurements are likely to be obtained if the test sample is prepared by grinding all of the original coal to pass the top size required, instead of screening the test sample out of a grind with some wider size distribution.

#### Acknowledgements

The authors would like to thank the UK Science and Engineering Research Council for their financial support under Grant No. GR/F 89817. The coal maceral analyses were measured by British Coal's Technical Services and Research Executive (TSRE) at Bretby. The TGA experiments were carried out at the British Gas plc London Research Station (LRS).

## References

1. Crelling, J.C., Southern Illinois University, Carbondale, personal communication.
2. Vorres, K.S., Energy & Fuels 4(5), 1990, 420-426.
3. Gibbins, J.R., King, R.A.V., Wood, R.J. and Kandiyoti, R., Rev. Sci. Instrum. 60, 1989, 1129-1139.
4. Man, C.K, Pendlebury, K.J. & Gibbins, J.R., ACS DFC Prepr. 37(1), 1992, 103-109.
5. Gibbins, J.R. & Kandiyoti, R., Energy & Fuels, 2, 1988, 505-511.
6. Littlejohn, R.F., J. Inst. Fuel, 39, 1966, 59.
7. Li, C.-Z., Gaines, A.F., Guell, A.J. & Kandiyoti, R., Proc. 1991 Int. Conf. on Coal Science, Newcastle, 1991, 723-726.

Table 1 Mass distributions from first grinding process

Coal	Size fraction, $\mu\text{m}$ (wt.%)				
	150-106	106-75	75-53	53-38	<38
Daw Mill	18.8	19.2	18.2	11.8	32.0
Kellingley	15.8	60.2	19.2	4.8	n/a
Pittsburgh #8	12.6	17.0	16.1	10.3	44.0
SB vitrain	26.2	22.0	17.1	22.5	12.2

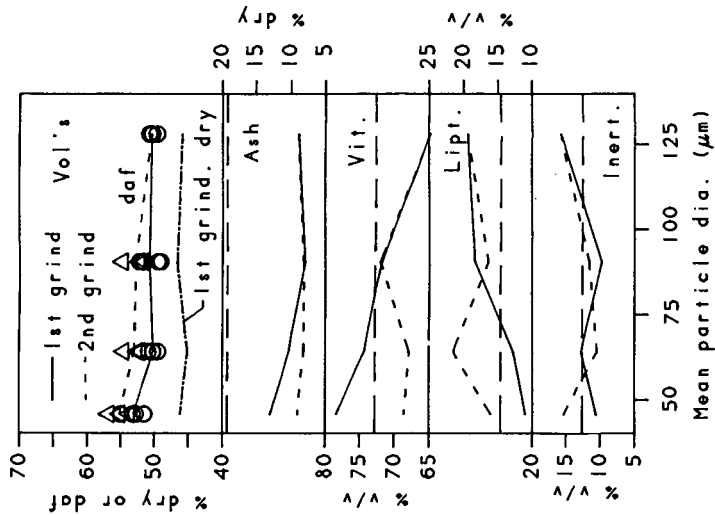


Fig. 1 Daw Mill coal - variation in volatile yields and mineral and maceral enrichment with size fraction.

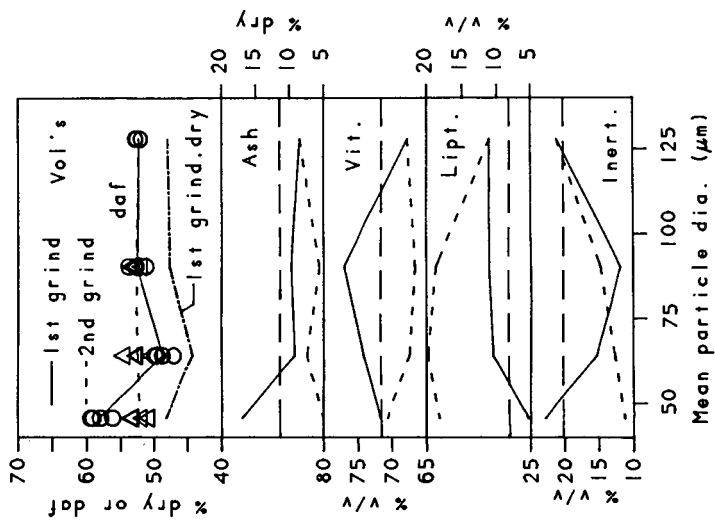


Fig. 2 Kellingley coal - variation in volatile yields and mineral and maceral enrichment with size fraction.

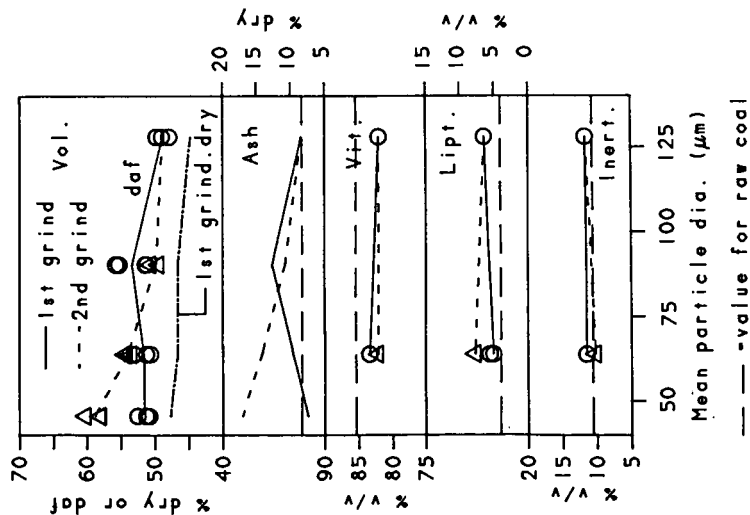


Fig. 3 Pittsburgh No. 8 coal - variation in volatile yields and maceral enrichment with size fraction.

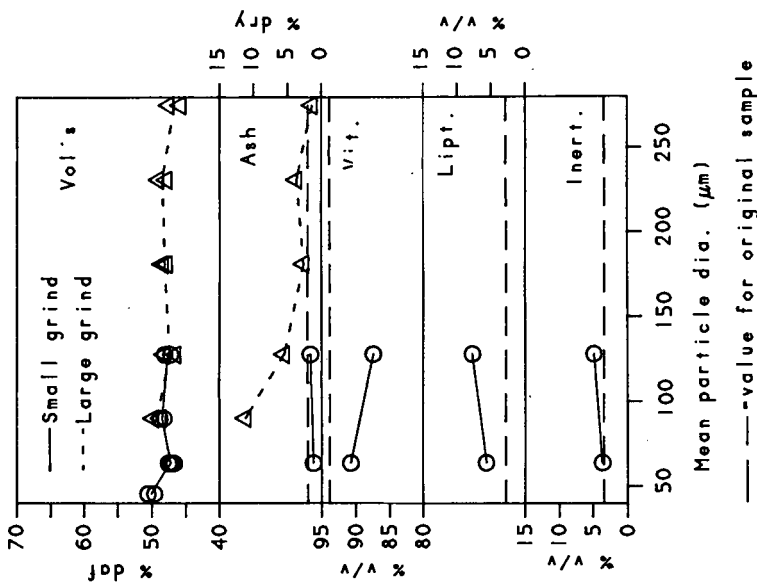


Fig. 4 Shirebrook Blackstone vitrain - variation in volatile yields and maceral enrichment with size fraction.

## THE INFLUENCE OF CHAR STRUCTURE ON LOW TEMPERATURE COMBUSTION REACTIVITY

S. Charpenay, M.A. Serio, H. Teng, and P.R. Solomon  
Advanced Fuel Research, Inc., 87 Church Street, East Hartford, CT 06108

**Keywords :** char structure, combustion reactivity, pore diffusion

### INTRODUCTION

Coal char is a porous material with a structure which is intimately related to its combustion properties. In particular, the internal structure influences the degree of intraparticle diffusion limitations present at various temperatures. For fluid coals, the char structure is expected to depend on the extent of "reorganization" during the fluid stage, and should vary with the pyrolysis heating rate, the pyrolysis temperature and the holding time. On the other hand, coals which do not become fluid should produce chars with a structure similar to that of the original coal. It has been shown in a previous study<sup>1</sup> that the pyrolysis heating rate has an impact on the reactivity of fluid chars. Since reactivity was measured in the kinetic regime, this effect should not be related to the char physical structure, except for differences in internal surface area. However, the extent of rearrangement during the period when the char is fluid may well affect both the physical pore structure and the molecular order. The latter quantity will determine the active site concentration. In that previous study<sup>1</sup>, the reactivity of low rank coals was found to be relatively independent of the time-temperature history, as long as the same degree of pyrolysis is reached. This is consistent with the fact that no important structure reorganization is expected to occur with these non-fluid coals.

The current study investigated the influence of the starting coal type (softening or non-softening) and of the char formation conditions on the onset of the pore diffusion regime. The reactivity of chars produced from fluid coals at different heating rates, and from non-fluid coals at low heating rate was measured isothermally with a TGA. Cumulative pore volumes and nitrogen surface areas were measured in order to be correlated with the behavior of the chars towards pore diffusion limitations.

The transition from zone I (kinetic regime) to zone II (combination of pore diffusion and kinetic regime) has been observed in a TGA apparatus by several researchers<sup>2,3,4,5</sup>. The chars studied were, in all cases, produced at low heating rate, i.e., a few degrees per minute. Tseng and Edgar<sup>2,3</sup> observed variations in the activation energy for lignite chars (from approximately 28 kcal/mol in the kinetic regime to 14 kcal/mol in the pore diffusion regime) and anthracite and bituminous coal chars (from about 33 kcal/mol to 22 kcal/mol). For an identical particle size of 650  $\mu\text{m}$ , their results show that the lignite chars reach the pore diffusion regime at a much higher reaction rate (roughly an order of magnitude) than the bituminous or anthracite chars. This implies that the structure of the lignite char is probably more "open", thus retarding diffusion limitations. The values of the  $\text{N}_2$ -BET surface areas at 0% burnoff were measured and were found to be of the order of 100  $\text{m}^2/\text{g}$  for the lignite char, 15  $\text{m}^2/\text{g}$  for the bituminous char and 1-2  $\text{m}^2/\text{g}$  for the anthracite char. These values are consistent with the assumption of a more porous structure for the lignite chars. Su and Perlmutter<sup>4</sup> studied chars produced at different heating rates (in the range 1 to 10 K/min), for different pyrolysis temperatures (873 to 1223 K) and for

different starting coals (anthracite and bituminous coals). They concluded that chars with different pore structures can be generated from the same coals by varying pyrolysis conditions: a higher final pyrolysis temperature or a slower heating rate generate chars of more compact structure. Floess et al.<sup>5</sup> compared the behavior of a microporous sucrose char with a macroporous spherocarb char and observed that the reactivity of the former varied with particle size, while the latter did not display such an effect. They attributed the difference in behavior to the different structure of the chars (purely microporous versus microporous and macroporous), and in particular to the presence of large microporous domains in the sucrose char. As Hurt et al.<sup>6</sup> pointed out, the degree of meso and macroporosity defines the size of the microporous regions, and consequently influences the degree of diffusion limitations in the micropores. In other words, for highly meso/macroporous chars, where the microporous regions are small, the micropores may not be diffusion limited before the meso/macropores themselves. This situation is similar to the one described in Thiele<sup>7</sup> where, even if most of the reaction occurs in small micropores, the meso/macropores configuration is assumed to control intraparticle diffusion. Walker<sup>8</sup> and Simons<sup>9</sup> arrived at the same general conclusion, although using different approaches. Consequently, it is important to estimate the degree of micro and meso/macroporosity of a char in order to predict the degree of pore diffusion limitations.

In order to assess differences in pore structures, multiple techniques such as gas adsorption (for surface areas and pore size distribution measurements), helium pycnometry (densities) and mercury intrusion (macropores distribution) can be used. White et al.<sup>10</sup> performed a comprehensive study on representative US coal chars (from lignite to bituminous) in order to determine surface area, pore size and volume distribution, and density. The chars were prepared at high heating rate in a flat flame burner (in the presence of oxygen), which is representative of char formation in pulverized coal combustion processes. They observed large variations in properties between the original coals and the corresponding chars: increase by two to three-fold for CO<sub>2</sub>-DP surface area, by 20-200-fold for N<sub>2</sub>-BET surface area, by 5-10-fold for pore volume, by three to four-fold for porosity. However, the differences between the chars produced from different coals were not very important, and varied by less than a factor of 2 for surface area, less than a factor of 2 for pore volume, and less than 15% for porosity. All of the chars were fairly porous (porosity of about 0.6-0.7) with most of the pore volume in macropores, and had N<sub>2</sub> surface areas of about 100-200 m<sup>2</sup>/g and CO<sub>2</sub> surface areas of about 200-500 m<sup>2</sup>/g.

More significant variations between the chars studied in the present work were expected, due to the widely different char formation conditions used.

## EXPERIMENTAL

**Coal Samples** - The coals used are from the Argonne Premium Coal Sample Program. The original coal particle size fraction is -100 mesh.

**Char Preparation** - The chars prepared in the TGA were produced by heating at 30°C/min in helium up to the pyrolysis temperature. In the case of non-fluid, non-agglomerating chars, the isothermal combustion cycle was done immediately after the pyrolysis cycle (without removing the sample from the TGA). In that case, the coal sample size was approximately 10 mg, which corresponds to a char sample of 4 to 7 mg. For fluid coals, since the particles have agglomerated during low heating rate pyrolysis, the char was prepared in larger quantity (150 mg) and was separated into different size fractions. The char average particle size was measured with an ISI Scanning Electron Microscope. The same procedure was applied to the char

prepared in an entrained flow reactor (EFR).

**Isothermal Reactivity Measurements** - The reaction rates at low temperatures were measured isothermally using a Dupont 951 TGA. The reaction rate is constantly monitored during the entire burnoff process. All experiments were performed using an oxygen partial pressure of 17.2 kPa, a total flow rate of 240 cc/min, and a char sample size of 4 to 10 mg. For the chars prepared in advance in the TGA or the EFR, the char sample was heated under a helium atmosphere at 30°C/min up to the combustion temperature, and the oxygen was introduced after 15 minutes to allow equilibrium.

**Nitrogen Adsorption Measurements** - Adsorption isotherms in nitrogen were obtained using the dynamic, continuous flow method. The measurements were made using a Quantasorb instrument (Quantachrome Corp.). From the adsorption isotherm, the cumulative pore volume was calculated. The nitrogen surface areas were obtained using the BET equation (single point).

## RESULTS AND DISCUSSION

**Reactivity Measurements** - Chars from the fluid coal Pittsburgh No. 8 were produced at low heating rate in a TGA (Pitts8 TGA) and at high heating rate in an entrained flow reactor (Pitts8 EFR). In order to evaluate the influence of coal rank on pore structure, a char from a Zap lignite was also produced at low heating rate in the TGA (Zap TGA). A char from a demineralized Zap was produced under the same conditions for comparison (Zapd TGA). Table I gives a summary of the properties of the chars studied.

Isothermal measurements of reactivity were obtained for each char over a wide range of temperature, which covered usually 3 orders of magnitude in reactivity. The reported rate was taken at 35% burnoff in all cases, in order to avoid any uncertainty in the calculation of the reaction rate because of the relatively high weight increase due to oxygen adsorption at lower burnoff levels. As shown in Fig. 1, a leveling off of the rate is observed for all chars at a rate of approximately 1 g/g.min. This behavior is due to external mass transfer resistances in the TGA, and would not occur under typical pulverized coal combustion conditions. The Zap TGA char was also found to ignite, which is indicated by the presence of a discontinuity in the reactivity.

As shown in Fig. 1, at low temperature all the chars studied indicated a similar activation energy, which fell in the range of 28 to 34 kcal/mol. The Arrhenius plots for the low heating rate, fluid char Pitts8 TGA showed a gradual change in activation energy, from approximately 28 kcal/mol at low temperature, to 22 kcal/mol at higher temperature. This behavior is observed for the two different particle sizes studied, 150  $\mu\text{m}$  and 800  $\mu\text{m}$ . Following the Thiele<sup>7</sup> model, the observed change in activation energy is believed to represent the transition from regime I (kinetic) to regime II (pore diffusion). However, features relative to the effect of particle size in each regime need to be clarified. In particular, the fact that, at low temperature (i.e. in the kinetic regime), the 150  $\mu\text{m}$  particle size presents a reactivity higher than the one from the 800  $\mu\text{m}$  particle size requires some explanation. This phenomenon has been observed by other researchers<sup>5,11</sup>. van Heek and Mühlen<sup>11</sup> proposed that the enrichment of product gases inside the larger particles caused by too small diffusion coefficients or too large flow resistances is responsible for the inhibition of the reaction rate. On the other hand, at higher temperatures (in the pore diffusion regime), the variation in rate between the two size fractions is smaller than expected: since the two particle sizes differ by about a factor of 5, the same factor should be obtained between the reaction rates. However, only a factor of 2 is found. A possible explanation of this effect may

result from finding out where the diffusion limitations take place in the particle. If we consider the char to be formed by microporous grains (or regions) surrounded by meso or macropores, diffusion limitations can occur either in the grains (if these are large) or in the meso/macropores (in the case of small microporous grains). In other words, for a char with large microporous regions, the diffusion parameter  $D_{\text{micro}}/L_{\text{micro}}^2$  (where  $D_{\text{micro}}$  is the effective diffusivity and  $L_{\text{micro}}$  is the diffusion distance in the microporous grains) is lower than the corresponding parameter  $D_{\text{meso/macro}}/L_{\text{meso/macro}}^2$  for the meso/macropores, where  $L_{\text{meso/macro}}$  represents a distance of the order of the particle size. In such a case, particle size effects may not be present, or would be weak, until the particle size is small enough (i.e. of the size of the microporous regions), in which case the diffusion distance is effectively reduced. The fact that a very low  $N_2$  surface area of  $0.5 \text{ m}^2/\text{g}$  at 0% burnoff is found for that char would also be consistent with this assumption, since it implies that few meso and macropores are present. In such a case, the microporous regions could be fairly large.

In contrast with the low heating rate char, Pitts8 TGA, the char produced at high heating rate Pitts8 EFR, did not show much change in activation energy (i.e. did not reach the pore diffusion regime) before entering the external diffusion limitation regime. Its  $N_2$  surface area (at 0% burnoff) was also found to be higher ( $4 \text{ m}^2/\text{g}$  versus  $0.5 \text{ m}^2/\text{g}$ ) than the one from Pitts8 TGA. This behavior is consistent with the findings of Su and Perlmutter<sup>4</sup> that low heating rate chars have a more compact structure. The lignite and demineralized lignite chars Zap TGA and Zapd TGA behaved similarly to the Pitts8 EFR. Their surface areas ( $84 \text{ m}^2/\text{g}$  and  $100 \text{ m}^2/\text{g}$  respectively) were also much higher than the ones from either of the Pittsburgh No. 8 chars.

**Pore structure characterization** - In an attempt to characterize the pore structure of the chars studied, nitrogen adsorption measurements were performed. Nitrogen adsorption is done at the temperature of liquid nitrogen (77 K). Adsorption is assumed to occur in the mesopores but not in the micropores (at least in the case of 0% burnoff chars) because of activated diffusion. However, since the micropores open up at higher burnoffs, those also adsorb nitrogen in the case of partially combusted chars.

The  $N_2$  adsorption data at 0% burnoff provide useful information on the number and accessibility of the mesopores of the char. Since mesopores probably constitute the main pathway for oxygen to penetrate into the particle, their characterization is an important step in order to predict diffusion limitations. Fig. 2 shows the adsorption isotherms for the Pitts8 EFR and the Pitts8 TGA at 0% burnoff. Pitts8 EFR char produces an isotherm of type IV (characteristic of the presence of pores in the transitional range) while Pitts8 TGA produces an isotherm of the types II or III (non porous). Also, the adsorbed volume is larger in the case of the Pitts8 EFR than for the Pitts8 TGA. The adsorption isotherm for Zap TGA char is shown in Fig. 3, and is characteristic of a porous material with numerous mesopores. Fig. 4 gives the cumulative pore volume for the three chars. These results confirm, in the case of the high heating rate Pitts8 EFR, the presence of more mesopores than in the low heating rate Pitts8 TGA char and are consistent with the assumption that the latter possesses larger microporous regions than the former. Also, as expected, the structure of the Zap TGA char is much more porous than the chars from the fluid coals. This is consistent with the results from Tseng and Edgar<sup>2,3</sup> who found that for the same particle size, a bituminous char entered the diffusion limited regime before a lignite char. A more quantitative correlation of the pore volume with the degree of diffusion limitations will require additional data in the pore diffusion limited regime for the highly porous chars.

It is well known that the  $N_2$  adsorption pattern changes significantly after a few percent of burnoff.

In order to evaluate those variations, Pitts8 TGA and the Pitts8 EFR chars were produced at 10% and 35% burnoff respectively. Although the degree of burnoff of the two chars is different, it can be reasonably assumed that the internal structure does not vary significantly between 10 and 35% burnoff. The combustion temperature was chosen to be sufficiently low as to be in the kinetic regime. Under these conditions, the pore structure is expected to vary uniformly through the whole particle. It should be noted that this may not be how the structure changes when burnoff is performed at higher temperature, i.e., in the pore diffusion regime (in that case burnoff occurs mostly at the exterior of the particle, with the interior not being modified). Fig. 5 presents the adsorption isotherm for the Pitts8 TGA at 10% burnoff and the Pitts8 EFR at 35% burnoff. The two chars produce an adsorption isotherm characteristic of a microporous structure<sup>12</sup>, with most of the pores being smaller than about 20 Å. In that case, the Kelvin equation cannot be utilized to calculate the pore size distribution. The value of the  $N_2$  surface area also increased dramatically, from 0.5 to 98 m<sup>2</sup>/g for the Pitts8 TGA char and from 4 to 310 m<sup>2</sup>/g for the Pitts8 EFR. These results indicate that the structure of both coal chars is mostly microporous. However, the degree of meso and macroporosity (which is important to estimate for transport processes) cannot be evaluated easily from these measurements. Also, since the burnoff was performed in the kinetic regime, it does not give a representation of the structure obtained when the combustion is done under more severe conditions. Additional data from chars combusted at high temperatures (i.e. in the pore diffusion regime) is needed. This point will be addressed in more detail in a future publication.

## CONCLUSIONS

From this study it can be concluded that low heating rate, fluid chars are less macroporous than high heating rate, fluid chars or lignite chars. This conclusion is consistent with the observation that the low heating rate, fluid chars enter the pore diffusion regime earlier than the other chars. It was also shown that char structural parameters such as surface area and cumulative pore volume can be correlated with the behavior of the char towards pore diffusion limitations. However, additional data obtained in the pore diffusion regime is necessary in order to establish a quantitative correlation between structural properties and the onset of diffusion limitations for a wide range of chars.

## ACKNOWLEDGEMENT

The authors are grateful for the support of the Morgantown Energy Technology Center of the United States Department of Energy under contract DE-AC21-86MC23075, for support of the study of char reactivity. The authors wish to acknowledge the contributions of Marie DiTaranto of Advanced Fuel Research to the experimental work, and helpful discussions with Prof. Suuberg of Brown University.

## REFERENCES

1. Serio, M.A., Solomon, P.R., and Bassilakis, R., ACS Div. Fuel Chem. Preprints, 34 (1), (1989)
2. Tseng, H.P., Edgar, T.F., Fuel, 63, 385, (1984)
3. Tseng, H.P., Edgar, T.F., Fuel, 64, 373, (1985)
4. Su, J.L., Perlmutter, D.D., AIChE J., 31, 973, (1985)
5. Floess, J.K., Longwell, J.P., Sarofim, A.F., Energy and Fuels, 2, 18-26, (1988)
6. Hurt, R.H., Sarofim, A.F., Longwell, J.P., Energy and Fuels, 5, 290-299, (1991)
7. Thiele, E.W., Ind. Eng. Chem., 31, 916, (1939)

8. Walker, P.L., Fuel, 59, 809, (1980)
9. Simons, G.A., Combustion Science and Technology, 20, 107-116, (1979)
10. White, W.E., Bartholomew, C.H., Hecker, W.C., Smith, D.M., Adsorption Science and Technology, vol.7, No.4, 180, (1990)
11. van Heek, K.H., Mühlen, H.J., in "Fundamental Issues in control of carbon gasification Reactivity", J. Lahaye and P. Ehrburger (Eds), Kluwer Academic Publishers, 1-34, (1991)
12. Gregg, S.J., Sing, K.S.W., Adsorption, Surface Area and Porosity, 2nd Edn, Academic Press, New York, (1982)

**TABLE I Char Properties**

Char	Coal	Reactor	Heating Rate (°C/s)	Final Temp.(°C)	Char Particle Size (μm)	N <sub>2</sub> Surface Area (m <sup>2</sup> /g)
Pitts8 TGA	Pitts 8	TGA	0.5	900	800 ± 200* 150 ± 50	0% BO:0.5 10% BO:98
Pitts8 EFR	Pitts 8	EFR	5000	1100	130 ± 30	0% BO:4 35% BO:310
Zap TGA	Zap	TGA	0.5	900	80 ± 40	0% BO:84
Zapd TGA	Zap	TGA	0.5	900	60 ± 20	0% BO:100

\* In that case, the combustion cycle was performed immediately after the pyrolysis. The particle size is approximate, since the chars showed a cenospheric agglomerated structure.

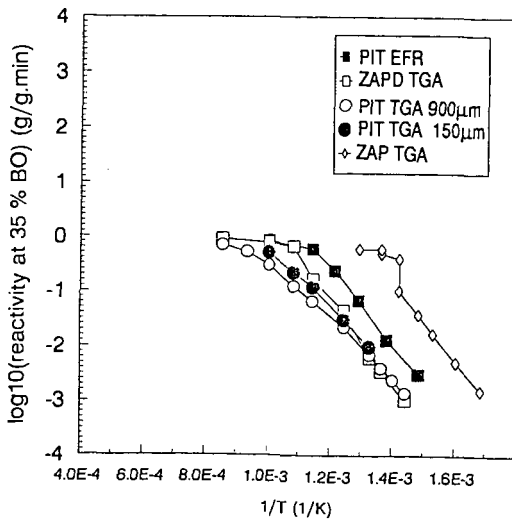


**Figure 1.** Measured Reactivity at 35% Burn-off of PITTS8 TGA, PITTS8 EFR, ZAP TGA, ZAPD TGA Chars as a Function of 1/T.

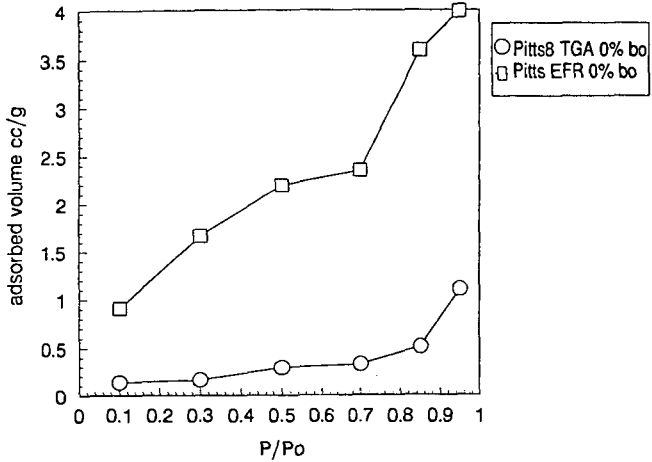


Figure 2. Nitrogen Adsorption Isotherms for PITTS8 EFR and PITTS8 TGA Chars.

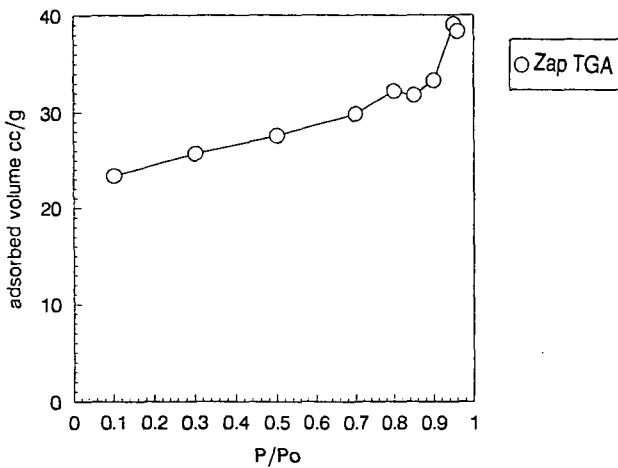


Figure 3. Nitrogen Adsorption Isotherm for ZAP TGA Char.

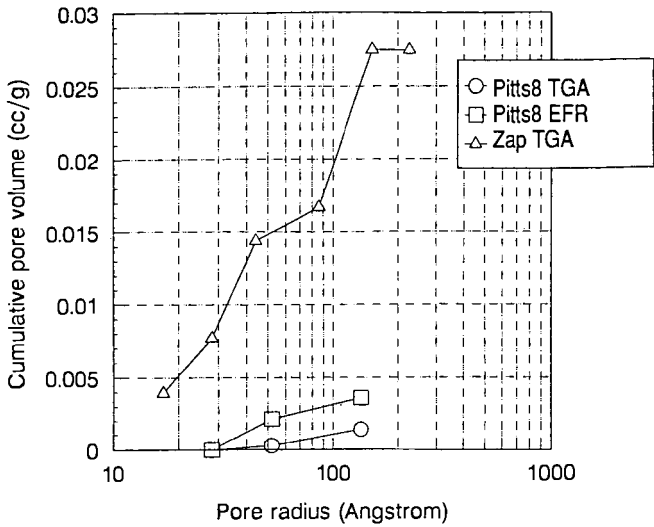


Figure 4. Cumulative Pore Volume for PITTS8 EFR, PITTS8 TGA and ZAP TGA Chars.

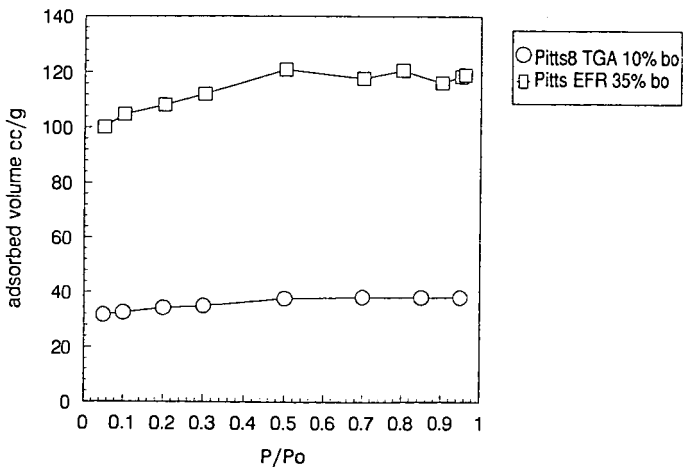


Figure 5. Nitrogen Adsorption Isotherms for PITTS8 EFR at 35% Burn-off and PITTS8 TGA at 10% Burn-off.

## GAS EVOLUTION FROM COAL IN SEALED GLASS AMPOULES\*

K. S. Vorres  
Chemistry Division, Building 211, Argonne National Laboratory  
Argonne, IL 60439, USA

### INTRODUCTION:

Earlier publications reported studies on the gas content of Argonne Premium Coal Samples (1,2). These samples are available in ampoules of 5 grams of -100 mesh and 10 grams of -20 mesh. They were periodically opened in vacuum and analyzed with a mass spectrometer as part of a quality monitoring program. The samples were originally sealed under nitrogen in a glove box maintained at less than 40 ppm of oxygen. Moisture present in the coal was kept in the samples as much as possible. Determinations of the gases were made and provide an opportunity to observe the changes due to transformations, release of dissolved gases or other processes in the samples. Changes in the gas content were observed and may be useful in interpreting a variety of phenomena.

The eight Argonne Premium Coal Samples are described below:

#	Name	Rank	State	Dmmf C	Dmmf H	Abbrev.
1	Upper Freeport	MVB	PA	88.08	4.84	UF
2	Wyodak-Anderson	SUB	WY	75.01	5.42	WY
3	Illinois #6	HVB	IL	77.67	5.20	IL
4	Pittsburgh	HVB	PA	83.20	5.43	PITT
5	Pocahontas #3	LVB	VA	91.05	4.48	POC
6	Blind Canyon	HVB	UT	80.69	5.81	UT
7	Lewiston-Stockton	HVB	WV	82.58	5.44	WV
8	Beulah-Zap	LIG	ND	74.05	4.90	ND

LVB = Low volatile bituminous, MVB = Medium volatile bituminous, HVB = High volatile bituminous, SUB = subbituminous, LIG = Lignite, State = U. S. A. State of origin, Dmmf = dry mineral matter-free, Abbrev = Abbreviation used later

### EXPERIMENTAL:

The Argonne premium coal samples have been sealed in borosilicate glass ampoules in a nitrogen atmosphere (3). A hydrogen-oxygen torch was used for the sealing. The hydrogen and oxygen gas flows were controlled with a gas mass flow controller to maintain stoichiometric conditions during the sealing. The oxygen content of the glovebox system was constantly monitored during the operation and no significant deviations from the expected values were observed.

\*This work was supported by the Office of Basic Energy Sciences, Division of Chemical Sciences, U. S. Department of Energy, under contract number W-31-109-ENG-38.

A supply of coal ampoules for each of the eight samples in each of the two mesh sizes was selected to provide samples for analysis over several years at initial sample consumption rates of about two per year. The ampoules were sent to the Analytical Chemistry Laboratory of the Argonne National Laboratory for gas analysis. The ampoules were placed in an evacuable chamber and the surrounding air was pumped out. A magnetic hammer was used to break the ampoule and release the atmosphere above the ampoules.

For the measurements until 1991, the gas was passed into a Consolidated Engineering Corporation (CEC) model 21-620 mass spectrometer and analyzed for nitrogen, methane, carbon dioxide, hydrogen, argon, water vapor, and higher hydrocarbons. Carbon monoxide could not initially be distinguished from nitrogen and was not reported. A VG Gas Analysis mass spectrometer, model 30-01 equipped with electron multiplier detector, was obtained in 1990 to replace the CEC unit and provide better data. Carbon monoxide can now be detected in the nitrogen, and lower limits of detection exist for the oxygen measurements.

The data obtained are condensed in Table I below.

Table I. Methane and Carbon Dioxide Concentrations in Argonne Premium Coal Sample Ampoules.

Coal	major gas	-100 mesh				-20 mesh			
		CH <sub>4</sub> max.	time	CO <sub>2</sub> max.	time	CH <sub>4</sub> max	time	CO <sub>2</sub> max	time
UF	CH <sub>4</sub>	+ .40	79	+ .13		P .70	79	+ .15	
WY	CO <sub>2</sub>	P- .02	63	P- .93		P .02	63	+ 1.4	
IL	CO <sub>2</sub>	P- .23	65	P- .23		P- .46	65	0 .66	
PITT	CH <sub>4</sub>	P- .8	64	P- .58		P- 14.5	64	0 3.7	
POC	CH <sub>4</sub>	P 1.2	62	+ .78		P- 7.6	62	P 5.1	
UT	CO <sub>2</sub>	P- .03	61	+ .10		0 .02	61	P .37	
WV	CO <sub>2</sub>	P- .03	59	+ .13		P- .23	59	0 .53	
ND	CO <sub>2</sub>	P- .02	58	+ 2.68		0 .03	58	P 3.3	

major gas = gas at higher concentration in ampoule (other than N<sub>2</sub>), trend = trend of changes in concentration (+ = increasing, 0 = constant, - = decreasing, P = plateau before or after trend), P- = decrease after plateau, max conc = maximum concentration of gas in ampoule in %, time = maximum time since sealing in months for data.

The data were plotted as concentration of gas versus time since sealing of the ampoules. Representative plots are shown in Figures 1-4. Figure 1 gives the concentration of CH<sub>4</sub> versus time since sealing for -100 mesh material. Figure 2 gives a similar

plot for the -20 mesh material. Figure 3 gives the concentration of CO<sub>2</sub> versus time since sealing for -100 mesh material, while Figure 4 provides similar information for the -20 mesh material.

#### RESULTS AND DISCUSSION:

Differences in the gas contents were observed as time passed. Considerable amounts of methane were released during the initial size reduction in the sample processing facility. The gas contents in Table I represent subsequent gas releases. Lower rank (Beulah-Zap and Wyodak-Anderson) and some intermediate rank (Illinois #6, Blind Canyon, Lewiston-Stockton) ampoules contained more carbon dioxide, while several higher rank (Pocahontas #3, Upper Freeport, Pittsburgh seam) ampoules contained more methane. In most cases, if carbon dioxide contents increased then methane contents did not increase, and vice-versa. Oxygen contents remained at or below the limits of detection, indicating the integrity of the ampoules.

The data in Figure 1 indicate the variation in methane for the six most concentrated -100 mesh samples. In general, the concentration increases as the time since sealing increases. The highest rank coal, Pocahontas, shows the largest methane concentration. The next highest rank, Upper Freeport, has a lower methane concentration than the Pittsburgh seam (lower rank in this group). A comparison in a similar plot for -20 mesh particles for these three coals indicates the highest concentration for the Pittsburgh seam followed by the Pocahontas and Upper Freeport in that order. The data are more limited but show an increase with concentration with time. The maximum concentration for the Pittsburgh seam coal was about 14% of the gas volume, or more than an order of magnitude greater than for the -100 mesh material. For early measurements

The data in Figure 3 indicate the carbon dioxide content of the gas space in the ampoules above the -100 mesh lower rank samples. The Beulah-Zap sample (legend ND) clearly released the most carbon dioxide at 2.6%. The Wyodak-Anderson sample released the next largest amount with the concentration increasing almost linearly over time. A similar plot of releases from -20 mesh material indicated that the evolution was only about 50% larger for the Beulah-Zap material. The values for the other coals were two to three times as high. The concentrations for the remaining samples were Pittsburgh > Illinois #6 > Lewiston-Stockton (legend WV) > Blind Canyon (legend UT). The latter three were relatively constant for the period in which the samples were analyzed.

The data in Figure 4 for -20 mesh samples indicate that the carbon dioxide concentrations are higher than those for the -100 mesh samples. This behavior is consistent with that observed for the methane measurements from the different particle sizes. The more striking difference is that the concentrations in the Pocahontas and Pittsburgh samples have increased to exceed that from the Beulah-Zap sample.

It is believed that the gas is dissolved in the coal matter and is released very slowly. Bacterial activity is not considered responsible since either carbon dioxide or methane but generally

not both are released from the samples, as might be expected from many bacterial actions. The most recent data indicate that significant quantities of carbon monoxide are not released in that the concentrations are at or below the limits of detection (.02%).

#### CONCLUSIONS:

1. Higher rank coals evolve methane, and lower rank coals evolve carbon dioxide with some evolution of both gases for the intermediate ranks.
2. The evolution proceeds over times of years for pulverized coals in sealed ampoules.
3. Gas concentrations are higher above -20 mesh samples than above -100 mesh material.
4. Carbon monoxide is not evolved.
5. The Wyodak sample evolves carbon dioxide approximately linearly with time.
6. The gas evolution seems to be associated with evolution of dissolved species.

#### ACKNOWLEDGMENTS:

The author expresses his grateful appreciation to A. Engelkemier for her analyses of the coal ampoule atmospheres. Gratitude is also expressed to the U. S. Department of Energy, Office of Basic Energy Sciences, Chemical Sciences Division for support.

#### REFERENCES:

- (1) Vorres, K. S., Proc. 1989 Intl. Conf. on Coal Science, Vol. II, 1083 (1989).
- (2) Vorres, K. S., Proc. 1991 Intl. Conf. on Coal Science, Vol. I, 147 (1991).
- (3) Vorres, K. S., The Argonne Premium Coal Sample Program, Energy & Fuels, 1990, 4, 420-426.

Fig. 1, Six Highest -100 Mesh Methane

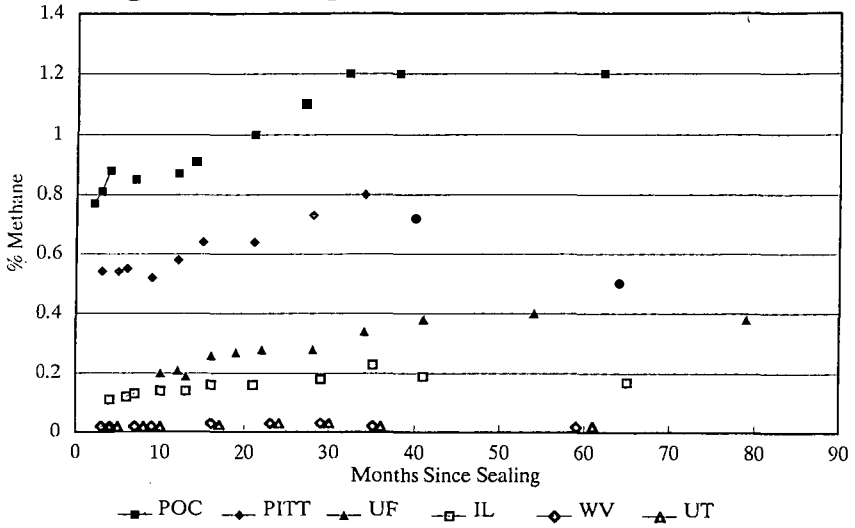


Fig. 2, Six Highest -20 Mesh Methane

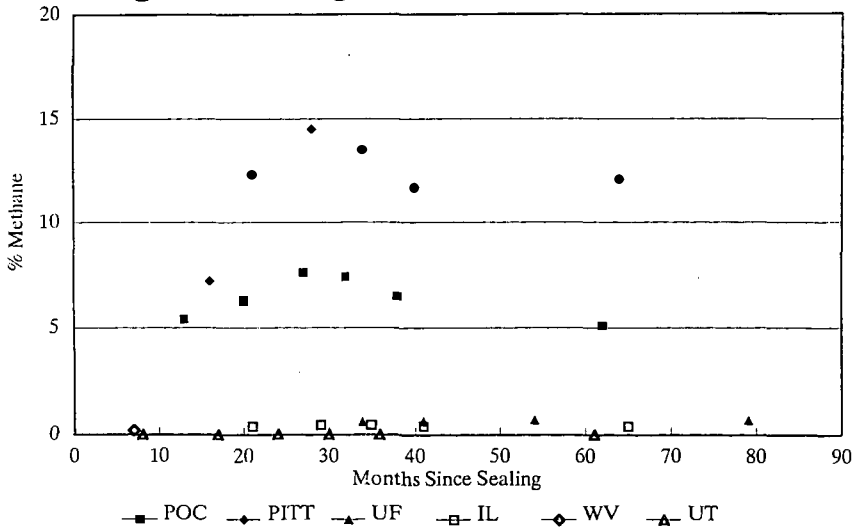


Fig. 3, Six Highest -100 Mesh CO2

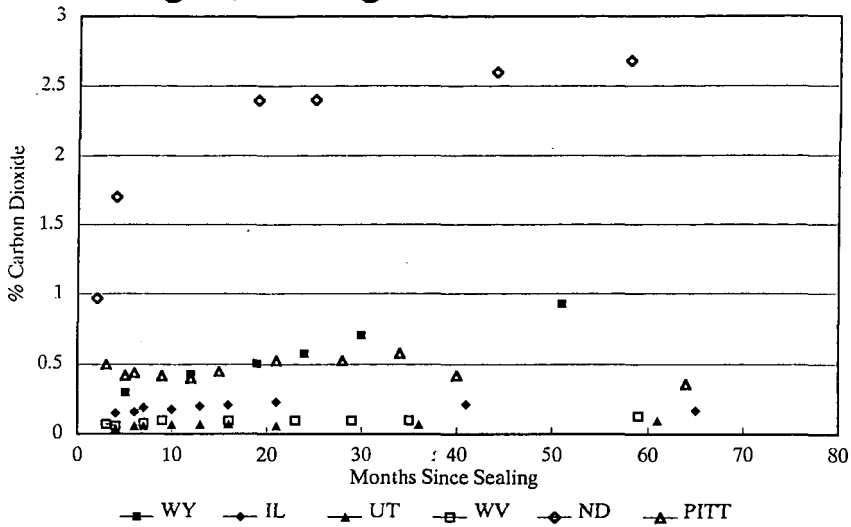
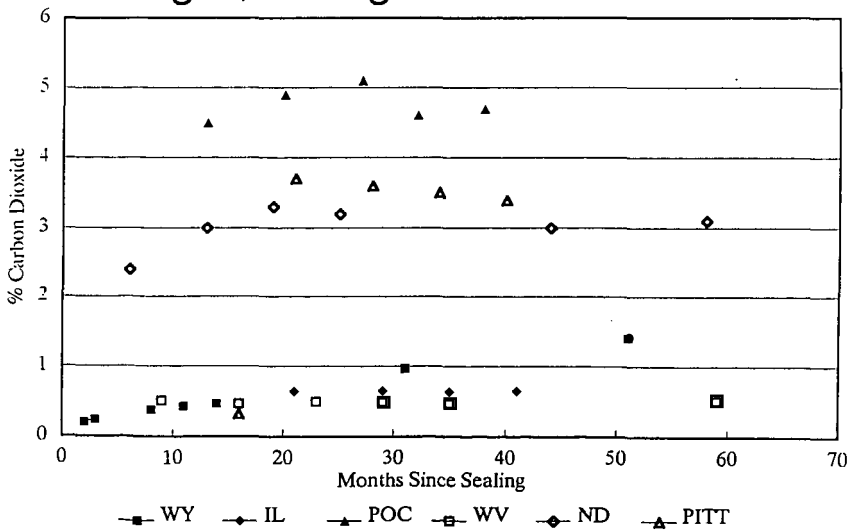


Fig. 4, Six Highest -20 Mesh CO2



## HYDROGASIFICATION OF BROWN COAL WITH ACTIVE IRON CATALYSTS FROM FERRIC CHLORIDE

Kenji Asami and Yasuo Ohtsuka  
Research Center for Carbonaceous Resources  
Institute for Chemical Reaction Science  
Tohoku University, Sendai 980, JAPAN

**Keywords:** Coal, Hydrogasification, Iron Catalyst

### INTRODUCTION

It would be necessary nowadays that coal is converted into the environmentally acceptable fuels. Gasification of coal with hydrogen is an important process for producing clean SNG. Since the reaction rate is very slow, high temperature and high pressure are required in the absence of catalyst [1], and thus an active and inexpensive catalyst should be developed. Iron is one of the most promising catalysts for the hydrogasification of coal. We have been trying to utilize acid wastes from metal pickling and titanium oxide production plants as Fe catalyst sources, because the wastes are cheap and abundant. When Fe chlorides or sulfates of the major components are added onto coal by the conventional impregnation method, they are inactive for the gasification in  $H_2$  at low temperatures [2], and Cl- or S-containing gases evolved during gasification may result in serious problems such as corrosion. However, we have recently found that Cl-free Fe catalysts finely-dispersed on low-rank coals can be successfully prepared from an aqueous solution of  $FeCl_3$  using several additives, and exhibit high activities for the low temperature gasification with steam [3,4].

In the present work, these Fe catalysts are applied to the gasification of brown coal in atmospheric  $H_2$  at low temperatures below 1200 K. The relationship between the catalytic activity and the preparation method and the catalytic state is examined.

### EXPERIMENTAL

**Coal and Catalyst.** Australian Loy Yang brown coal with a particle size of 0.15 - 0.25 mm was employed in this study. The proximate analysis was ash, 0.5; volatile matter, 52.4; fixed carbon, 47.1 wt% (dry), and the ultimate analysis was C, 66.7; H, 4.6; N, 0.5; S, 0.3; O, 27.9 wt% (daf).

Three kinds of Fe catalysts were precipitated onto brown coal from an aqueous solution of  $FeCl_3$  with different additives, that is, urea  $((NH_2)_2CO)$ ,  $Ca(OH)_2$ , and  $NH_3/NH_4Cl$  buffer solution. These catalysts are abbreviated as Fe(U), Fe(C), and Fe(A), respectively. In the preparation of Fe(U), urea was added to the mixture of coal and  $FeCl_3$  solution so that fine particles of  $FeOOH$  could be precipitated onto coal [5], and the resulting mixture was stirred at 370 K. For Fe(C) and Fe(A)  $Ca(OH)_2$  powder and  $NH_3/NH_4Cl$  solution were added instead of urea, respectively, and the aqueous mixture was stirred at room temperature. After each precipitation, the solution was filtered off, and the Fe-bearing coal was washed with deionized water repeatedly to remove the  $Cl^-$  or  $Ca^{+2}$  ions. The preparation methods have been described in detail elsewhere [3,4].

**Hydrogasification.** Gasification runs were isothermally conducted in a thermobalance under atmospheric  $H_2$  at 873-1173 K. Since all the samples were quickly heated up to a predetermined temperature, the coal devolatilization first took place, and after the completion within a few minutes char gasification started. The activity of Fe catalyst in the latter stage will be discussed throughout the paper. The reactivity of char after devolatilization is expressed by using both char conversion on a dry ash free and catalyst free basis and the specific rate of char, that is, the gasification rate per unit

weight of remaining char.

**X-ray diffraction.** X-ray diffraction (XRD) measurements of Fe-bearing coals and chars were made with Mn-filtered Fe-K $\alpha$  radiation to clarify the chemical form and dispersion state of Fe catalyst. The average crystallite size of Fe species was determined by the Debye-Schörrer method.

## RESULTS AND DISCUSSION

**Catalyst Components.** The actual Fe loading of each sample was 3.4, 4.7, and 4.6 wt% for Fe(U), Fe(C), and Fe(A), respectively. The chlorine content determined by a standard Eschka method was nearly equal to that in the original coal (0.08 wt%) in every catalyst, indicating the complete removal of Cl ions from FeCl<sub>3</sub> with water washing. A small amount of Ca<sup>2+</sup> (0.5 wt%) from Ca(OH)<sub>2</sub> was retained with Fe(C).

**Catalytic Activity for Hydrogasification.** Table 1 shows char conversion after 30 min in the hydrogasification at 873 K. The enhancement of the gasification rate by Fe catalyst was observed only in the early period of reaction, though not so high, and all the catalysts seemed to lose the activity in the latter stage. Char conversion showed that the order of the catalytic effectiveness was Fe(A) < Fe(C) < Fe(U).

Figure 1 illustrates the change in char conversion with reaction time at 1073 K. Every catalyst promoted the gasification, and the effectiveness was strongly dependent on the preparation method. The order of the activity was Fe(A) < Fe(U) < Fe(C), which is the same order as observed in the steam gasification [4]. With the most active Fe(C) char was completely gasified within about 100 min. The conversion at 120 min with Fe(U) and Fe(A) increased from 18 % without iron to 52% and 37%, respectively. Figure 2 shows the specific gasification rate as a function of char conversion at 1073 K. The rates for Fe(A) and the original coal were low and almost constant. The initial rates for Fe(U) and Fe(C) were almost the same, and they were about 20 times that without iron. The specific rate for Fe(U) decreased steeply with increasing conversion. On the contrary, the rate for Fe(C) increased gradually as the gasification proceeded. This rate increase was also observed at 1173 K. The change in specific rate with conversion may be determined by the balance between catalyst agglomeration and enrichment due to the consumption of char. When the catalyst enrichment is predominant as in the K-catalyzed gasification [6], the specific rate would increase with increasing conversion. The rate increase observed in the latter part of gasification with Fe(C) may be this case.

Thus, it is found that these precipitated Fe catalysts, especially Fe(C), exhibit high activities for the gasification of brown coal in atmospheric H<sub>2</sub> even at a temperature as low as 1073 K.

**Catalyst State.** Since no XRD lines of Fe species were detectable for each catalyst, the chemical form of Fe catalyst on coal could not be identified. However, other analytical techniques such as elemental analysis, ESCA, and FT-IR suggested that the catalyst exists as finely dispersed FeOOH [3,4].

The catalyst state immediately after devolatilization in H<sub>2</sub> at 873 K is summarized in Table 1. Major XRD species were  $\alpha$ -Fe irrespective of the catalyst type. Small peaks due to cementite (Fe<sub>3</sub>C) were also observed for Fe(C). The degree of catalyst dispersion evaluated from the average crystallite size of  $\alpha$ -Fe increased in the order of Fe(A) < Fe(C) < Fe(U). This order corresponded to that of the gasification activity, which suggests that the dispersion may be a key factor determining the catalytic effectiveness in this temperature region.

Figure 3 shows the XRD patterns for Fe-bearing chars devolatilized at 1073 K. When the devolatilization temperature was raised from 873 K to 1073 K, the main species for Fe(C) changed from  $\alpha$ -Fe to Fe<sub>3</sub>C and strong XRD lines of unidentified iron carbides

appeared with small signals of  $\alpha$ -Fe for Fe(U), whereas the major species for Fe(A),  $\alpha$ -Fe, remained unchanged, though weak peaks of unidentified carbides were observed. As is seen in Figure 1, Fe(C) was the most active catalyst at 1073 K, and it achieved the complete gasification of char. Although Fe<sub>3</sub>C is not always the actual active species because of the bulk chemical form identified by XRD, these observations suggest that the formation of iron carbide, perhaps Fe<sub>3</sub>C, may be essential for such the high activity in the temperature region of around 1100 K. In other words, the hydrogasification may proceed through the carbon dissolution mechanism [7,8]. On the other hand, the hydrogen spill-over mechanism [1,9] might be predominant in the Fe-catalyzed hydrogasification in the temperature region of around 850 K.

## CONCLUSIONS

Hydrogasification of brown coal with Cl-free Fe catalysts precipitated from FeCl<sub>3</sub> solution using different additives is carried out at ambient pressure. The activity depends strongly on the preparation method and the gasification temperature. The use of urea as an additive seems to give the most effective catalyst at 873 K. The iron prepared with Ca(OH)<sub>2</sub> shows the largest rate enhancement at 1073 K, and realizes complete gasification within a short time. The formation of Fe<sub>3</sub>C may be related to the catalytic activity in this case.

## ACKNOWLEDGMENTS

Ms. Naoko Yoshida and Ms. Naomi Katahira are gratefully acknowledged for their assistance in carrying out experiments. This work was partly supported by a Grant-in-Aid for Scientific Research from the Ministry of Education, Science and Culture, Japan (Nos. 0245082 and 03203204).

## REFERENCES

- [1] D.W. McKee, *Chem. Phys. Carbon*, **16**, 1 (1981).
- [2] Y. Ohtsuka, Y. Tamai, and A. Tomita, *Energy & Fuels*, **1**, 32 (1987).
- [3] Y. Ohtsuka and K. Asami, *Ind. Eng. Chem. Res.*, **30**, 1921 (1991).
- [4] K. Asami and Y. Ohtsuka, submitted to *Ind. Eng. Chem. Res.*
- [5] K. Kaneko, S. Ozeki, and K. Inouye, *J. Chem. Soc. Jpn.*, **1985**, 1351.
- [6] M.J. Verra and A.T. Bell, *Fuel*, **57**, 194 (1979).
- [7] C.W. Keep, S. Terry, and M. Wells, *J. Catal.*, **66**, 451 (1980).
- [8] W.L. Holstein and M. Boudart, *J. Catal.*, **72**, 328 (1981).
- [9] E. Keren and A. Soffer, *J. Catal.*, **50**, 43 (1977).

Table 1 Activity and state of Fe catalysts at 873 K.

Sample	Additive	Conv. <sup>a)</sup> (wt%)	Chem. form <sup>b)</sup>	Size <sup>b),c)</sup> (nm)
Fe(U)	(NH <sub>2</sub> ) <sub>2</sub> CO	20	α-Fe	10
Fe(C)	Ca(OH) <sub>2</sub>	13	α-Fe, (Fe <sub>3</sub> C)	28
Fe(A)	NH <sub>3</sub> /NH <sub>4</sub> Cl	8	α-Fe	45
Original	—	5	—	—

a) Char conversion after 30 min.

b) Immediately after devolatilization in H<sub>2</sub>.

c) Average crystallite size of α-Fe.

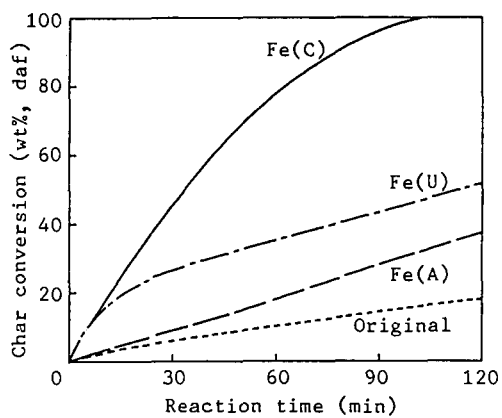


Figure 1 Hydrogasification of Loy Yang coal with iron catalysts at 1073 K.

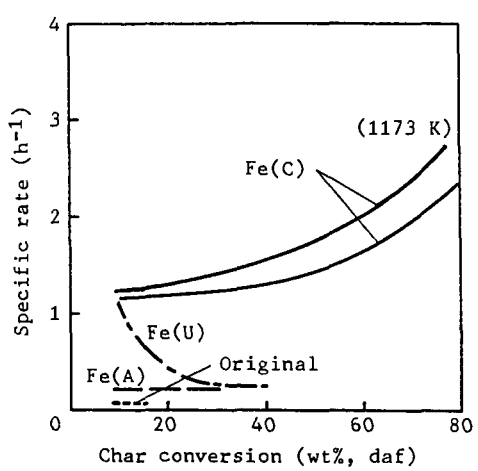


Figure 2 Profiles of specific gasification rates at 1073 K.

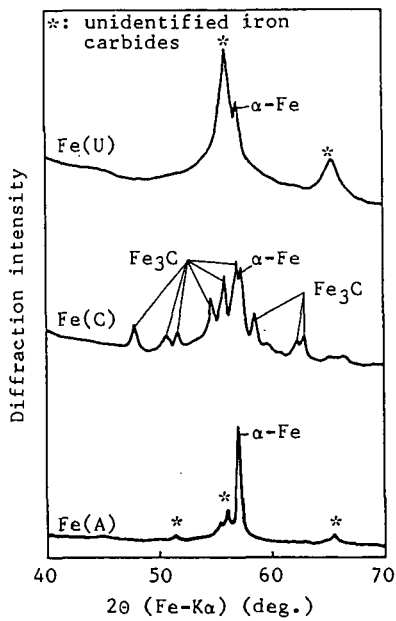


Figure 3 XRD patterns of iron catalysts on the chars devolatilized at 1073 K.

## THE CATALYTIC ACTIVITY OF Fe/ZSM-5 FOR HYDROCARBON SYNTHESIS AND EXAFS STUDY OF ITS STRUCTURE

Qiwu Wang, Shiqiang Wei and Minming Huang

Department of Modern Chemistry, University of Science and Technology of China, Hefei, Anhui, P. R. China

Keywords: Fe/ZSM-5, Hydrogenation, EXAFS

### INTRODUCTION

Hydrogenation of carbon dioxide has been paid more and more attention recently because of its green house effect and for synthesis of hydrocarbons and alcohols<sup>1,2</sup>. Unfortunately, it was observed that carbon dioxide can be converted into only carbon monoxide and methane over the many effective Fisher-Tropsch catalysts. The selectivities forming more than C<sub>2</sub> hydrocarbons and alcohols on them are, if any, very low<sup>3</sup>. In the recent years, Fe, Rh and other catalysts supported on suitable carriers and having some promoters were found to have high selectivities for C<sub>2</sub>-C<sub>4</sub> hydrocarbons under high pressures<sup>4,5</sup>. Some studies of adsorption of CO<sub>2</sub> by IR and the catalytical reaction kinetics under different temperatures and pressures were also reported<sup>6,7</sup>. All these researches have given great contribution to develop the catalytic conversion process of carbon dioxide to match the requirement of human environment protection and new energy source.

In this paper it is reported that the Fe/ZSM-5 has good selectivity to C<sub>2</sub>-C<sub>4</sub> in the hydrogenation of CO<sub>2</sub> and EXAFS study shows the change of the local environment of Fe on the catalyst during the deactivation process.

### EXPERIMENTAL

Preparation of catalysts: The weighed amount of metal nitrate, such as 2.93 g ferric nitrate, was dissolved in water to make a diluted solution in which 5.0 g support, HZSM-5 zeolite, was added. It stands in room temperature for two hrs by frequently stirring and dried at 393K for 10 hrs. The impregnated precursor was calcined at 723K, 2 hrs in flow of 40 ml/min of air, and cooled to room temperature to get the oxidized state of

the catalyst, 7.5% Fe/ZSM-5. It was reduced in a stainless steel reactor in hydrogen at 773K, for 4 hrs before hydrogenation of CO<sub>2</sub>.

**Hydrogenation:** The activity of the catalysts was determined in a flow system at space rate, 6000 ml/g.h with CO<sub>2</sub>:H<sub>2</sub>=1:4 at different temperatures between 500 to 650K and under 1-20 atmospheric pressures. The products were analyzed by a gas chromatographic system with HFD and TCD as detectors for hydrocarbons and the gases.

**X-ray absorption:** The X-ray absorption experiments were performed on Rigaku, 6KVA anode-rotating X-ray machine. The photon intensity was recorded with a solid detector and TP-801 monitor. All data analysis was carried out with EXAFS program on IBM-PC computer. The fitting was done using experimentally determined Fe-O and Fe-Fe phase shifts and backscattering amplitudes.

## RESULTS AND DISCUSSION

### 1. The effects of supports on activity and selectivities

The same amounts of Fe, such as 15%, were supported on SiO<sub>2</sub>, Al<sub>2</sub>O<sub>3</sub>, HZSM-5, Cr<sub>2</sub>O<sub>3</sub>, Nb<sub>2</sub>O<sub>5</sub> and La<sub>2</sub>O<sub>3</sub> individually by impregnation, calcination and then reduction at 773K, in H<sub>2</sub>, for 4 hrs. The hydrogenation activity and selectivities were measured in the flow system at 600K, 6000 ml/g.h of the reactant mixture of CO<sub>2</sub>:H<sub>2</sub>=1:4. The activity expressed as the percentage of conversion of CO<sub>2</sub> and the selectivities as percents of the converted CO<sub>2</sub> are listed in Table 1. From the data it can be seen that the properties of supports affect conversion of CO<sub>2</sub> very seriously, HZSM-5 made the Fe catalyst active 50 time more than that on La<sub>2</sub>O<sub>3</sub> and the selectivity forming C<sub>2</sub>+C<sub>3</sub> can reaches to 33.2% on Fe/ZSM-5, only about 1% on Fe/SiO<sub>2</sub>, Fe/Al<sub>2</sub>O<sub>3</sub> and Fe/Cr<sub>2</sub>O<sub>3</sub> and even nothing on Fe/La<sub>2</sub>O<sub>3</sub>. The better effect of Nb<sub>2</sub>O<sub>5</sub> on the C<sub>2</sub>+C<sub>3</sub> selectivities is in agreement with that reported in the literature<sup>8</sup>.

### 2. Loading of Fe on HZSM-5 and its effects on catalytic properties

The results listed in Table 2 indicate that the activity and C<sub>2</sub> and C<sub>3</sub> selectivities gradually increase by loading more and more Fe until 30% on the support. XRD experiments demonstrate that the increasing loading of

Fe resulted in the growing up of Fe particles on the reduced catalysts from 170 to 310Å (average particle diameter) from 5 to 30% Fe on HZSM-5. It can also be seen from Table 2 that the changes of C<sub>2</sub> and C<sub>3</sub> selectivities parallel with each other for loading more Fe and rising reaction temperatures. These results show that the metal Fe surface plays the main role in the hydrogenation of carbon dioxide and for growing of the C-C chains. In this particle size range, the larger, the particle of metal Fe, the better, the catalytical reactivity.

### 3. The effects of some promoters

Addition of 2.5% Cu, Ni, Ru, Rh, Co, the easily reduced metals to 15%Fe/ZSM-5 increase the activity and C<sub>2</sub>, C<sub>3</sub> selectivities at high reaction temperatures. At 650K the conversion of CO<sub>2</sub> reached 30.1% over Fe-Ru/ZSM-5 and CO, CH<sub>4</sub>, C<sub>2</sub>, C<sub>3</sub> and C<sub>4</sub> selectivities are 30.5, 27.7, 20.8, 14.0 and 7.0 respectively, that is, hydrocarbons become the main products, C<sub>2</sub>+C<sub>3</sub>+C<sub>4</sub>, 41.8% besides 27.7% CH<sub>4</sub> and CO only 30.5%. Promoter, Ni lets methane to be the main hydrogenation product, 51.5% in 4.1% converted CO<sub>2</sub> at 550K. However at 650K, C<sub>2</sub>+C<sub>3</sub> hydrocarbons reach to 21.7% , methane 22.9% and CO, 45.4% in 31.5 % converted CO<sub>2</sub>. As shown in the author's TPR experiments<sup>9</sup>, Ni and Ru could move the reduction peak temperatures of Fe<sub>2</sub>O<sub>3</sub> to the lower positions, that is, they could promote the reduction of Fe to metal state which is necessary to catalytical hydrogenation of CO<sub>2</sub> over Fe catalysts.

Na<sub>2</sub>O and MgO and other alkaline and alkaline earth metal oxides can increase a little bit of the hydrogenation activity, however, decrease the C<sub>2</sub> selectivity. They can inhibit the growing of C-C chain making methane as the main products<sup>10</sup>.

The transition metal oxides, such as V<sub>2</sub>O<sub>5</sub>, MoO<sub>3</sub> and Cr<sub>2</sub>O<sub>3</sub> decrease both the hydrogenation activity and C<sub>2</sub>, C<sub>3</sub> selectivities a lot at low reaction temperatures. In comparison with Fe/ZSM-5, these promoted catalysts have great temperature dependence. At 650K they have a comparable activity to that over Fe/ZSM-5 except the lower selectivities. These phenomena could be related to the inhibition effect to reduction of FeO and this effect would decline at the temperatures as higher as 650K.

### 4. Stability of the catalysts

In Fig.1 the hydrogenation activity and C<sub>1</sub>, C<sub>2</sub> and C<sub>3</sub> selectivities on Fe/ZSM-5, Fe-Cu/ZSM-5, Fe-Ru/ZSM-5, Fe-Cr/ZSM-5 and Fe-Cu-Ru/ZSM-5 were plotted against the reaction time. Although the initial activities on Fe/ZSM-5 and Fe-Cu/ZSM-5 are very high and reach the maxima after 1 hour, they drop very quickly later. After 5 hrs, the selectivities forming C<sub>1</sub>, C<sub>2</sub> and C<sub>3</sub> gradually decrease to the lowest values. On the contrary, the effect of Ru is very interesting. Over Fe-Cu-Ru/ZSM-5 the selectivities of C<sub>2</sub> and C<sub>3</sub> keep increasing with reaction time at expense of that of methane when the conversion of CO<sub>2</sub> gradually increases to a stable level, around 10%. After 10 hrs, selectivities of C<sub>1</sub>, C<sub>2</sub> and C<sub>3</sub> reach to 38.0, 19.0 and 16.5% respectively. It seems that the active centers which favor to growing of C-C chains were formed with reaction time instead of that for methane. The co-promoters, Cu-Ru, make Fe-Cu-Ru/ZSM-5 the best hydrocarbon synthesis catalyst from CO<sub>2</sub> and H<sub>2</sub> under our experimental conditions.

## 5. EXAFS study of the structure of the catalysts

EXAFS as a powerful tool has been widely used for study of the structure of catalysts.<sup>12</sup> The data obtained by fitting the filtrated  $k^2 \cdot x(k)$  with models of Fe-C and Fe-Fe for the Fe local environments of different catalysts at the different reaction times are listed in Table 3. The Radial Structure Functions (RSF) of Fe in Fe/ZSM-5 catalyst measured after 0.5, 2.0 and 24h are shown in Fig.2. It can be seen from Table 3 that the new Fe-C coordination was formed in the deactivated Fe- and Fe-Cu catalysts, the coordination numbers of nearest Fe around Fe centers decrease with time from 7.5 and 8.5 (0h) to 2.5 and 3.0 (24h) and a farther Fe-Fe formed.

From Fig.2 we can see that the peak height of Fe-Fe obviously decrease with time if we know the different Y-scales in the three figures from 40 (0h) to 20 (24h) being used and the large noise level in the third figure. The Fe-Fe interaction was interrupted by the carbon atoms which enter between iron atoms and some kind of Fe-C species are formed owing to the deposit of the carbon atoms on the surface during the reaction process. All these caused the deactivation of the catalysts. On Fe-Cu-Ru/ZSM-5, Fe-Fe coordination number almost does not change comparing 7.0 after 24h to 7.5 for 0h Fe/ZSM-5 and at the same time only 0.4 carbon atoms approach to Fe atoms on Fe-Cu-Ru/ZSM-5 comparing 2.5 on Fe/ZSM-5. It is known that Cu can inhibit the deposit of inactive carbon on Fe surface<sup>13</sup>. The better activity and stability of the Fe-Cu-Ru/ZSM-5 than

that of the others can be explained from the viewpoint of the local structure of Fe on the catalysts by EXAFS study.

#### Reference

1. Solymosi, F., Erdohelyi, A. & Bansagi, T.; *J. Catal.*, 68, 371 (1981)
2. Nozaki, F., Sodesawa, T. Satoh, S. & Kimura, K., *J. Catal.*, 104, 339 (1987)
3. Rehmat, A. & Randhava, S. S., *Ind. Eng. Chem. Prod. Res. Develop.*, 9, 512 (1970)
4. Lee, M. D., Lee, J. E. & Chang, C. S., *Bull. Chem. Soc. Japan*, 62, 2756 (1989)
5. Trovarelli, A., Mustazza, C. & Dolcetti, G., *Appl. Catal.*, 65, 129 (1990)
6. Solymosi, F. & Knozinger, H., *J. Catal.*, 122, 166 (1990)
7. Peebles, D. E., Goodman, D. W. & White, J. M., *J. Phys. Chem.*, 87, 4378 (1983).
8. Weatherbee, G. D. & Bartholomew, C. H., *J. Catal.*, 68, 67 (1981)
9. Wei, S., Huang, M., Chen, S., Rong, J., Wang, Q. & Yang T., *Chinese J. Chem. Phys.* 4, 303 (1991)
10. Compbell, T. K. & Falconer, J. L., *Appl. Catal.*, 50, 189 (1989)
11. Stockwell, D.M., Bianchi, D. & Bennett, C. D., *J. Catal.*, 113(1988)
12. Wang, Q. & Wei S., *J. Petrochemistry (Chinese)* 20, 500 (1991)
13. Anderson, R.B., "Catalysis IV", Chapter 2, ed. Emmett, P. H., Reinhold Pub. Corp. (1956)

Table 1 Effects of Supports on the Activity and Selectivities

Support	Conv. %	Selectivity, %				
		CO	CH <sub>4</sub>	C <sub>2</sub>	C <sub>3</sub>	C <sub>2</sub> +C <sub>3</sub>
SiO <sub>2</sub>	2.3	89.9	8.9	1.2	0.0	1.2
Al <sub>2</sub> O <sub>3</sub>	6.4	98.0	1.4	0.4	0.1	0.5
HZSM-5	15.1	43.6	23.2	14.8	18.4	33.2
Cr <sub>2</sub> O <sub>3</sub>	5.2	92.2	6.5	1.0	0.3	1.3
Nb <sub>2</sub> O <sub>5</sub>	5.4	74.6	17.9	4.3	3.2	7.5
La <sub>2</sub> O <sub>3</sub>	0.3	95.2	4.7	0.0	0.0	0.0

Table 2 The Effects of Loading of Fe

Content %	Temp. K	Conv. %	Selectivity %				
			CO	CH <sub>4</sub>	C <sub>2</sub>	C <sub>3</sub>	C <sub>4</sub>
1.0	600	1.5	97.0	3.0	0.0	0.0	0.0
	650	5.1	98.8	1.0	0.2	0.0	0.0
5.0	550	1.8	82.0	16.4	1.6	0.0	0.0
	600	6.4	83.7	12.4	3.1	0.8	0.0
	650	11.5	88.8	8.5	2.4	0.3	0.0
7.5	550	2.5	76.8	17.9	2.3	1.2	0.5
	600	6.8	73.1	16.8	5.3	2.6	0.7
	650	5.5	71.5	14.9	6.7	3.2	0.2
15.0	500	1.2	85.0	12.0	2.0	1.0	0.0
	550	3.9	60.0	21.6	6.8	7.6	6.4
	600	5.1	43.6	23.2	14.8	12.0	6.4
	650	30.5	65.1	16.0	9.6	6.8	1.9
30.0	500	1.5	79.6	9.6	3.4	5.4	2.0
	550	5.3	67.3	13.5	5.7	5.6	7.9
	600	25.7	42.6	17.4	13.0	12.8	14.2
	650	39.4	53.8	16.7	12.0	11.4	6.1
60.0	500	3.0	82.9	12.3	1.7	1.7	1.4
	550	11.9	58.5	15.7	8.4	10.5	8.9
	600	27.7	36.9	16.9	11.9	16.7	17.6
	650	35.7	63.2	14.5	9.4	8.3	4.6

Table 3 EXAFS Results of the Catalysts

Catalyst	Bond	Reaction Time (h)				
		0.0	0.5	2.0	24	
15%Fe	Fe-C	R	2.00	2.00	1.90	
		CN	0.5	1.5	2.5	
	Fe-Fe	R	2.49	2.51	2.55	2.48
		CN	7.5	6.0	5.0	2.5
	Fe-Fe	R			2.60	2.65
		CN			2.5	3.8
15%Fe,10%Cu	Fe-C	R	2.00	2.00	1.87	
		CN	0.7	1.5	2.0	
	Fe-Fe	R	2.50	2.52	2.50	2.48
		CN	8.5	7.5	4.0	3.0
	Fe-Fe	R			2.60	2.65
		CN			2.5	5.0
15%Fe,10%Cu 2.5%Ru	Fe-C	R	2.00	2.00		
		CN	0.3	0.4		
	Fe-Fe	R			2.5	2.5
		CN			8.0	7.0

Notes: All catalysts were supported on HZSM-5. The unit of R is Å. CN-coordination number.

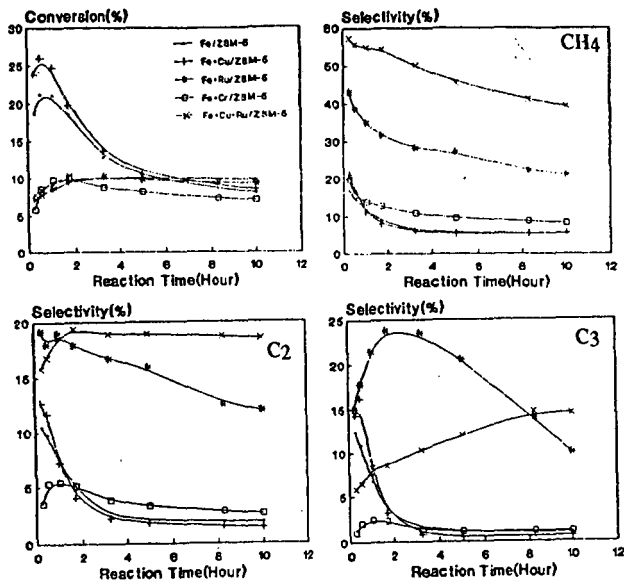


Fig.1 The relationship between the hydrogenation activity, selectivities and reaction time over several catalysts.

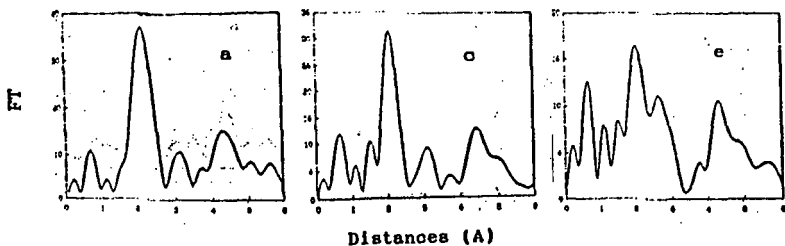


Fig.2 The RSFs of Fe measured at different reaction time. a-0.5h, b-2h and c-24h. The main peak at around 2.5Å is from the Fe-Fe coordination in Fe/ZSM-5.

## USE OF ACTIVATED COAL CHAR FOR REMOVAL OF VOLATILE ORGANIC COMPOUNDS FROM WATER

P. L. Beaulieu, S. M. Fatemi, and J. B. Tumidalsky, Analytical Research and Services Division, Amoco Research Center, Box 3011, Naperville, Illinois 60566, and  
C. W. Kruse, M. Chou, and C. Feizoulof, Illinois State Geological Survey, 615 East Peabody Drive, Champaign, Illinois 61820.

**Keywords:** char, environmental, adsorption, mild gasification, coal

### INTRODUCTION

Mild gasification is an alternative to traditional coal burning for coal utilization. Mild gasification produces gas, liquid, and substantial quantities of coke. Coal liquid and gas are being studied as alternatives to petroleum and natural gas, as sources of chemical feedstocks and fuels. This project concentrates on an alternate use for the solid coke, upgrading it to a higher value product, an activated char, and use for sorption of pollutants.

Activated charcoal is conventionally produced from a source such as coconut husk. We reported earlier on the conversion of coke to activated char by a process of controlled oxidation (1). There is a large market for activated charcoal as a sorbent for removal of organic compounds from water supplies and industrial outfalls. Presently, activated charcoal for this purpose is priced at more than \$1,000/ton. If coal char can successfully compete in this arena, the value of the coke would be upgraded dramatically, and the economics of coal utilization changed substantially. In this paper, we report on successful testing of activated coal char under laboratory conditions as a sorbent for removal of volatile organic compounds from deionized water.

Organohalogens are common environmental pollutants. We reported earlier that activated coal char catalytically promoted dehydrohalogenation and other elimination reactions, producing olefins (2-5). If an overall process of sorption of organic compounds from water and their catalytic decomposition and conversion to more useful or less noxious compounds can be demonstrated, it would represent an advantage for coal derived char over other charcoal types. Last minute results of experiments testing for decomposition of previously sorbed compounds will also be reported, if ready in time for the meeting.

### EXPERIMENTAL

Experimentation consisted of preparation of activated char from coal, equilibration with deionized water containing 37 organic compounds, and GC-MS analysis to measure the amounts of these compounds remaining in the water at the end of the sorption period. Details follow below.

**Preparation of Coal Char** Activated coal char was prepared from a blend of Illinois #5 (Springfield) and Illinois #6 (Herrin) coals using the following method. The starting material was char from a United Coal Company pilot scale, fixed bed, mild gasification reactor. This material was further devolatilized using a fluidized bed reactor at ISGS, heating in an atmosphere of pure nitrogen at a rate of 20°C/min, and holding a final temperature of 500°C for 15 minutes. After characterization, steam treatment followed. The material was heated at a rate of 20°C/min to 870°C in pure nitrogen. The atmosphere was changed to 50% steam in nitrogen, and conditions held constant for 3 hours to increase porosity. After characterization, mild oxidation followed. The material was heated at 20°C/min to 450°C in pure nitrogen. The atmosphere was changed to 10% oxygen in nitrogen, and conditions held constant for 15 minutes to activate the surface. This product, which had a surface area of 557 meter<sup>2</sup>/gram, was used for the sorption studies described below.

**Sorbates.** A methanolic stock solution of 37 analytes, each at 1000 ppm, was purchased from a vendor of environmental analytical standards (Accustandard). Components are listed in Table I. This solution contains most of the volatile organic compounds (VOC) for which federal and state discharge permits usually require screening. These are also known as VOA, for volatile organic analytes. Portions of this stock solution were injected (spiked) into water as described in the experiments detailed below.

**Equilibration Experiments.** Samples of char were covered with deionized water, and were either spiked immediately with the stock solution (Experiment 1), or spiked after a four hour conditioning period during which the char equilibrated with the unspiked water (Experiment 2). After spiking, the char was equilibrated with the spiked water for 20 hours (Experiments 1 & 2). Sampling of the water layer for GC-MS analysis followed. To do Experiment 3, several refilled samples from Experiment 2 were used. A second 20 hour equilibration and second GC-MS analysis followed. Experimental details follow.

**Experimental Details.** A sample of char (either 0.100 gram or 1.00 gram) was placed in a precleaned glass 40 milliliter environmental water sample vial (VOA vial). A second vial was designated immediately as control. Each was filled with deionized water and sealed immediately with its teflon faced septum screw cap. After the unspiked conditioning times described above, each vial was opened momentarily in turn, and a syringe (or glass micropipette) used to add a spike volume (0.002 to 1.00 milliliter) of the sorbate solution to each, injecting it well below the water surface. Taking care to exclude bubbles, the vial was resealed immediately and was mixed by inverting several times.

After the 20 hours spiked equilibration, the vials were sampled for GC-MS analysis. The deionized water needed for a dilution was placed in a VOA vial. Each vial was opened momentarily, and the volume for analysis removed. Except for the vials spiked with the smaller volumes, the aliquot taken was that required to prepare a diluted solution approximating 125 ppb in concentration. The volume was removed either by syringe (or glass micropipette) or by decanting and weighing (when the desired volume exceeded 5.00 milliliters). When a syringe (or glass micropipette) was used, this aliquot was injected below the surface of the deionized water in the analysis vial. When decanted, it was poured without vortex into the water in the analysis vial. For Experiment 3, the water volume removed for the GC-MS analysis in Experiment 2 was immediately replaced with fresh deionized water. The vials were immediately resealed, and equilibrated for 20 hours more. No makeup spike was added. This brought the cumulative equilibration time for Experiment 3 to 40 hours before the second sampling. Immediately after adding the sampled aliquot to the analysis vial, 0.080 milliliter of the internal standard and surrogate solution described below was added by micropipette, the vial topped up with deionized water, resealed and mixed. The resulting solution was analyzed by GC-MS as described below.

**Internal Standard Solution.** A combination solution of three internal standards (20 ppm each) and three surrogate analytes (25 ppm each) was prepared by diluting methanolic stock solutions (Accustandard, Supelco, or other vendor). High purity methanol was used as solvent. Internal standards are used as GC-MS references, for locating the chromatography peaks of the analytes, and for calculation of concentrations of analytes present. Surrogate analytes are used to ascertain that the GC-MS analysis and calculation methods are in control. Compounds used as internal standards and surrogates are listed in Table II.

**Method of Analysis.** Concentrations of the volatile analytes remaining in solution were measured by Purge and Trap GC/MS, using an automated version of EPA Method 8240, as was specified by EPA for analysis of waste water regulated under the Resource Conservation and Recovery Act (3). This method is largely the same as the earlier EPA Method 624 for sites regulated under the Clean Water Act (4). The analysis vials prepared as described above were placed in an autosampler, where they were held until a 5 milliliter volume was transferred automatically to the purge and trap device (OI Analytical 4460A). Helium was used to purge the volatile organics from the room temperature water sample, transferring the organic vapors to a multilayer (OV-1, Tenax, Silica Gel, Activated Charcoal) trap where they were held for analysis by GC-MS. On signal from the GC, the organic vapors were thermally desorbed and transferred to the GC, which was equipped with a 2 meter glass column (1% SP-1000 on 60-80 mesh Carbowax B). The temperature programmed GC sequentially eluted the components to the mass spectrometer over a period of about 40 minutes. The mass spectrometer was a Finnigan 4500 quadrupole instrument operating in the EI, positive ion, full scan mode. Scan time was 2 seconds, mass range 34 to 340 M/Z, and tuning was to EPA specifications for the spectrum for bromofluorobenzene.

Standard Finnigan peak search software was used to locate the chromatogra-

phy peaks, integrate the EPA recommended quantitation ion for each compound, and calculate results. To calculate results, the peak area for the analyte and that for the internal standard eluting nearest the analyte peak were obtained for a series of 5 calibration standards in the range 10-200 ppb. Relative response factors ("RRFs", relating analyte area, analyte concentration, internal standard area and internal standard concentration) were calculated. EPA statistical quality control requirements were followed in evaluating the analytical range, establishing initial average RRFs, and then for checking and updating the response factors to be used for calculation on a daily basis. Concentrations were then calculated in the analysis solutions using the library of daily RRFs.

#### GRAPHICAL PRESENTATION OF RESULTS

Most peaks for the 37 analytes were resolved, either by effective GC separation, or by identification of a unique quantitative mass. However, in the case of two peaks, each of which contained two isomers, resolution was not possible. This resulted in 35 calculated data points to be reported for each solution, including the sum peaks for the isomeric pairs. In addition to the 35 analytes, the three surrogate compounds were determined in the same manner. The amount of methanol was not determined. A value for the amount of each analyte (the  $i^{\text{th}}$  analyte) sorbed on the char was calculated as a percent, relative to the matching control solution, using the equation:

$$\text{Percent Sorbed } _i = 100 \times \frac{[\text{Concentration } _i \text{ in Control} - \text{Concentration } _i \text{ in Sample}]}{\text{Concentration } _i \text{ in Control}}$$

A typical component is illustrated in Figure I, where the data for benzene are shown. A total of 35 similar graphs resulted from the data processing. Several more graphs will be presented at the meeting, as germane to a discussion of the slight differences between sorption properties of the individual components and classes of components.

However, it proved easier to contrast and compare the data after further manipulation. The Average Percent Sorption was calculated for each sample from the percent sorption for the individual analytes in each sample/control pair. Average sorptions are shown in Figure II.

$$\text{Average Percent Sorption} = \frac{\sum_{i=1}^{35} \text{Percent Sorbed } _i}{35}$$

Figure III shows the relative strength of sorption listed by component. The sorption for benzene can be seen to closely resemble the average sorption. This was seen earlier by comparison of Figure I and Figure II, but the comparison is easier when Figure III is considered. This data for construction of Figure III was obtained by further calculation. Using the sample average sorption described for Figure II, the relative strength of sorption for each (that is, the  $i^{\text{th}}$ ) component in each sample was calculated using the equation:

$$\text{Relative Sorption Strength } _j = [\text{Percent Sorbed } _j - \text{Average Percent Sorption}]$$

The average relative sorption strength for this (the  $i^{\text{th}}$ ) component in for all ( $j = 17$ ) samples was then calculated and plotted in Figure III.

$$\text{Average Relative Sorption } _j = \frac{\sum_{j=1}^{17} \text{Relative Sorption Strength } _j}{17}$$

In Figure III, the analytes are listed alongside a bar graph representing the average sorptions of the analytes for all experiments. The analytes which sorb best are to the left of the vertical line. The center of the bar represents the average sorption over all experiments, the length of the bar is a measure of the precision (each bar is 2 standard deviations in length).

## DISCUSSION AND CONCLUSIONS

Fresh, dry Activated coal Char can be seen to have sorbed the analytes, with efficiencies improving at lower concentrations. Some individual analytes proved to be more strongly sorbed than others, and the strong sorbency persisted to higher concentrations.

The average results for Experiment 1, as presented in Figure I, will be considered first. In experiments at or below at 100 micrograms of each analyte per gram of char, removal was essentially complete for most analytes (96% sorption at the lowest concentration level studied, 50 ppb, leaving a concentration of only 2 ppb in solution). Above 100 micrograms of each analyte per gram of char, performance degraded. In the experiment at 5000 micrograms of each analyte per gram of char, removal of the sorbates from solution was largely incomplete (approximately 60% of all 35 analytes, at an aqueous concentration of 25 ppm, leaving 10 ppm in solution).

Results for the second (pre-soaked) experiment proved somewhat more variable and the char somewhat less effective. Most of the samples showed lower sorptions (for the same spike amount) than in the case of samples which were not pre-soaked. Two exceptions were noted to lie closer to the line representing the first experiment. These two are believed to represent samples which still contained entrained air. Note was not taken of samples which did not sink, and thus might still contain air, since this was not known to represent an important variable at the time. For the several samples refilled with deionized water, and allowed to reequilibrate with the spiked solutions, the amounts of each analyte sorbed increased.

Since presoaking with water was observed to degrade performance of the char somewhat, it is proposed that water binds active sites which would otherwise be available to the analytes. A hidden component, methanol, is probably also sorbing on the char, occupying active sites. If methanol is also sorbing, the total capacity of the char for organics is then probably much higher than the sum of the 37 analytes, but further work will be needed to measure the total capacity.

Kinetics have not been characterized at this point. In the presence of presoaked char, at a spike level of 50 micrograms of each analyte per gram of char, sorption appears to be approximately 60% complete in 20 hours and increases to the about 75% in 40 hours. Since the 40 hour equilibration never produced sorptions higher than those produced by the 20 hour equilibration with dry char, it is possible that the sorption is essentially complete by 20 hours in the presence of dry char, but further experimentation will be required to be certain.

In summary, activated coal char appears to be an effective sorbent for VOCs, but the equilibrium is displaced somewhat and/or the sorption rate slowed by presoaking the char in water.

## References:

1. C. W. Kruse, L. M. Lytle, M. Rostam Abadi, M. Chou, and Feizoulof (ISGS); S. M. Fatemi, J. A. Mahoney, P. L. Beaulieu, and J. O. Schreiner (Amoco) Annual Technical Report to the Center for Research on Sulfur in Coal, 1991. **Upgrading Mild Gasification Char: Evaluation of Oxidized Char as a Catalyst**
2. C. W. Kruse, G. C. Ray, U.S. Patent 3,240,834 Mar. 15, 1966.
3. J. E. Mahan, R. E. Reusser, C.W. Kruse, U.S. Patent 3,352,935 Nov.14 ,1967.
4. C.W. Kruse, U.S. Patent 3,437,695 Apr. 8, 1969.
5. C. W. Kruse, M. I. M. Chou, C. Feizoulof (ISGS); S. M. Fatemi, P. L. Beaulieu, J. O. Schreiner (Amoco); Vol 37#2, 556-563, 1992. 203rd ACS National Meeting, San Francisco, CA. **Evaluation of Oxidized Char as a Catalyst - I. Characterization**
6. United States Environmental Protection Agency; Office of Solid Waste & Emergency Response, Washington, D.C. 20460, November, 1986. **SW-846 Test Methods for Evaluating Solid Waste; Laboratory Manual; Physical/Chemical Methods; Volume IB; Third Edition.**
7. 40 CFR Part 136. United States Environmental Protection Agency **Guideline Establishing Test Procedures for the Analysis of Pollutants.**

**TABLE I. COMPONENTS OF SPIKE SOLUTION**

(each at 1000 Micrograms/Milliter, Except Methanol = Balance)

HALOGENATES		
C-1	C-2 (Unsat'd.)	C-3 (Unsat'd.)
Chloromethane	1,1-Dichloroethene	Vinyl Chloride
Bromomethane	Cis-1,2-Dichloroethene	Cis-1,3-Dichloropropene
Methylene Chloride	Trans-1,2-Dichloroethene	Trans-1,3-Dichloropropene
Bromodichloromethane	Trichloroethene	
Dibromochloromethane	Tetrachloroethene	
Chloroform		
Bromoform	C-2 (Sat'd.)	C-3 (Sat'd.)
Carbon Tetrachloride	Chloroethane	1,2-Dichloropropane
	1,1-Dichloroethane	
	1,2-Dichloroethane	
	1,1,1-Trichloroethane	
	1,1,2-Trichloroethane	
	1,1,2,2-Tetrachloroethane	
OXYGENATES		
Methanol (Solvent)	Acetone	
Vinyl Acetate	Methyl Ethyl Ketone (2-Butanone)	
	4-Methyl-2-Pentanone (MIBK)	
	2-Hexanone (MBK)	
AROMATICS		
Benzene	Ortho-Xylene	Styrene
Toluene	Meta-Xylene	Chlorobenzene
Ethylbenzene	Para-Xylene	
MISCELLANEOUS		
Carbon Disulfide		

**TABLE II. COMPONENTS OF INTERNAL STANDARD & SURROGATE SOLUTION**

SURROGATES		
1,2-Dichloroethane-D4	Toluene-D8	4-Bromofluorobenzene
INTERNAL STANDARDS		
Bromochloromethane	2-Bromo-1-Chloropropane	1,4-Dichlorobutane

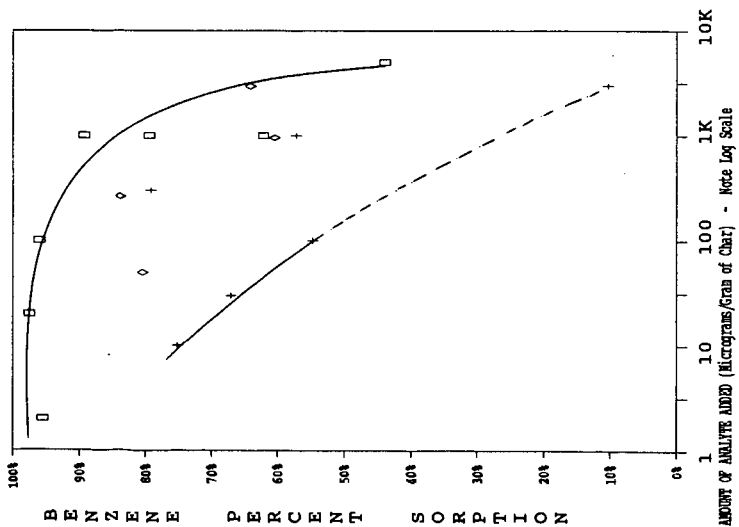


FIGURE 1. EFFECTIVENESS OF ACTIVATED COAL CHAR FOR REMOVAL OF BENZENE FROM WATER  
 ( ) Experiment 1. + Experiment 2. ◇ Experiment 3.

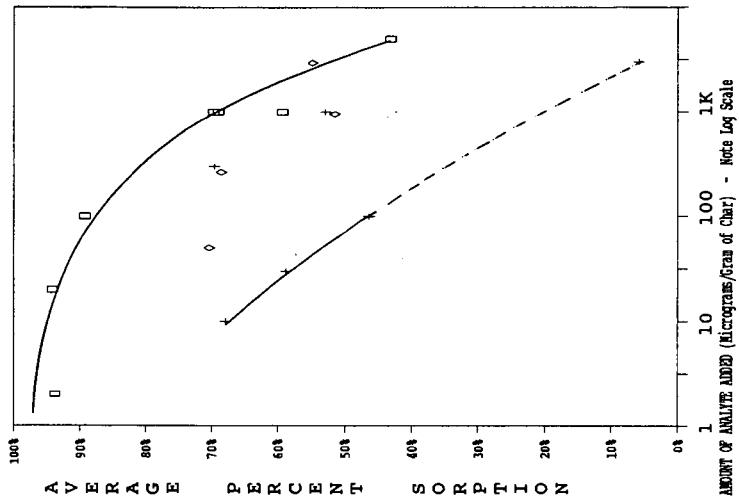
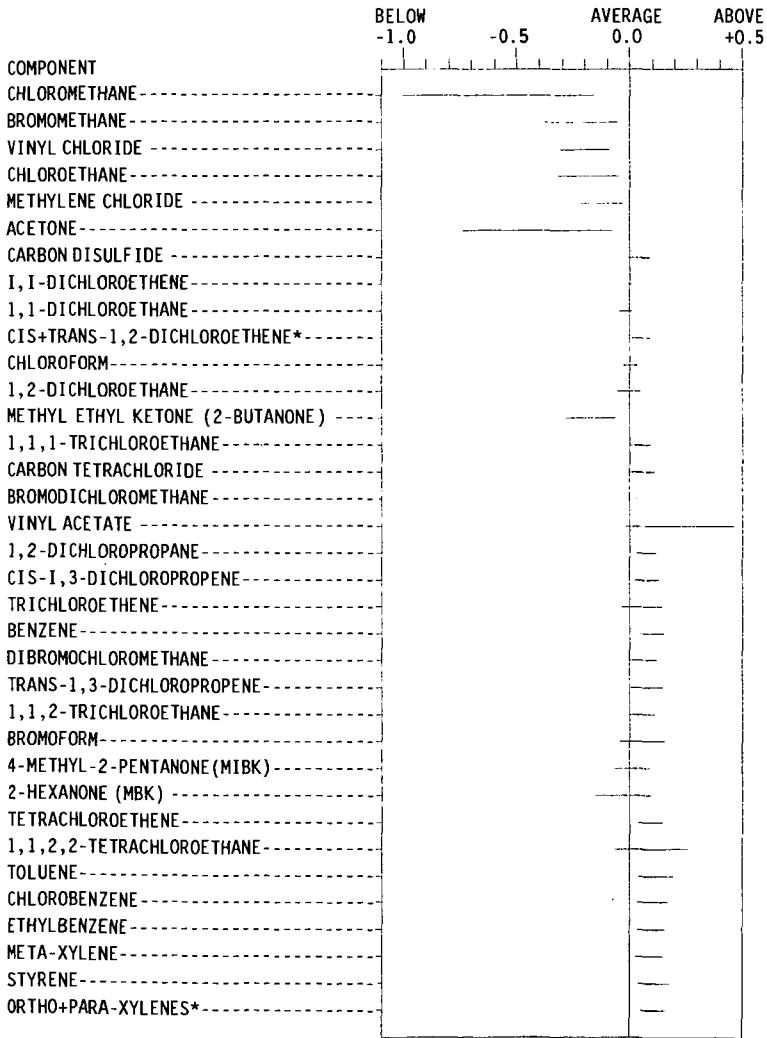


FIGURE 2. EFFECTIVENESS OF ACTIVATED COAL CHAR FOR REMOVAL OF VOC FROM WATER  
 ( ) Experiment 1. + Experiment 2. ◇ Experiment 3.

FIGURE III.

AVERAGE RELATIVE STRENGTH of SORPTION LISTED by COMPONENT



\* Coeluting Pair, quantified as single component